Shallow Geothermal Potential and Uncertainty Analysis of the Snake River Plain

Joseph Batir, Maria Richards, Matthew Hornbach, and David Blackwell
Southern Methodist University Geothermal Laboratory

and

Amanda Kolker
National Renewable Energy Laboratory

Submitted on December 31, 2020

Acknowledgments

This paper includes research contributions from Christine Ferguson and Sharon Fields, who work with the authors at the Southern Methodist University Geothermal Laboratory. Additional reviewers of this report include Al Waibel of Columbia Geoscience and two anonymous reviewers as part of the Geothermal Rising (previously Geothermal Resources Council) Annual Meeting paper submission process.

The work was performed by Southern Methodist University Geothermal Laboratory in collaboration with the National Renewable Energy Laboratory, upon funding from the Alliance for Sustainable Energy, LLC, Managing and Operating Contractor for the National Renewable Energy Laboratory for the U.S. Department of Energy, under Subcontract NO. XEJ-9-92239-01 under prime Contract NO. DE-AC36-08GO28308, and the Bureau of Land Management under Interagency Agreement L16PG00068/P0003. The views expressed in the article do not necessarily represent the views of the National Renewable Energy Laboratory or the U.S. Government.

List of Acronyms

BHT bottom-hole temperature

EGS enhanced geothermal systems

FORGE Frontier Observatory for Research in Geothermal Energy

GPFA Geothermal Play Fairway Analysis

INL Idaho National Laboratory

SMU Southern Methodist University

SRP Snake River Plain

- CSRP Central Snake River Plain
- ESRP Eastern Snake River Plain
- ESRPA Eastern Snake River Plain Aquifer
- WSRP Western Snake River Plain

USGS U.S. Geological Survey

Executive Summary

The Snake River Plain (SRP) terrestrial heat flow and subsurface thermal regime are important for assessing the local geothermal resource potential, both for conventional and enhanced geothermal systems (EGS) development in the region. Resource evaluation for the SRP is complicated by the disparate data density, along with the known lateral advection of heat in the Eastern SRP Aquifer (ESRPA) and vertical heat transport by fluids in the bounding faults, especially in the southwestern area and along the northeastern edge. This study produced increased resolution of the thermal regime of the Western SRP (WSRP) and a better understanding of the thermal regime controls in the greater SRP region. The data collection included 926 wells with at least temperature and depth data, and additional heat flow and lithology data from the National Geothermal Data System, the Idaho Oil and Gas Conservation Commission's database,[1] and the Southern Methodist University (SMU) Geothermal Lab Heat Flow database. After quality assessment, the final heat flow data set includes 206 data sites utilized for heat flow and temperature-at-depth calculations. This new data compilation includes available measurements from recent studies (e.g., the Snake River Plain Play Fairway Analysis, the Idaho Frontier Observatory for Research in Geothermal Energy [FORGE] site, and the *HOTSPOT* Project).

The SMU Geothermal Laboratory conducted detailed studies of the SRP tectonics and heat flow since the 1970s and as part of the EGS geothermal potential estimation for the conterminous United States in 2006 and again in 2011, calculating geothermal potential from 3.5 km to 10 km depth. Recent temperature modeling refined the calculation methodology to estimate shallow (1 km to 4 km) resource potential using an improved thermal conductivity model and incorporation of shallow groundwater flow. By incorporating the new SRP geology, geophysics, and 206 thermal data sites with the SMU thermal modeling methodology, this project updates the resource estimate for the SRP and generates new temperature-at-depth maps for the shallow subsurface (1 km to 4 km). The project results highlight the electrical potential resource areas (≥150°C) and areas with more exploration risks based on minimal and/or low-quality data.

From the results of this study, the total electrical thermal potential (>150°C) within 1 km to 4 km depths is approximately 44,000 MW_e. This power potential excludes non-development regions based on the National Renewable Energy Laboratory's non-development GIS layer, which removes areas that are not able to be developed such as urban infrastructure, zones protected under the roadless area conservation rule, high slope angle terrain, lakes, rivers, and others. Estimated temperatures above 150°C are as shallow as 1.6 km depth, and known temperatures above 150°C are measured starting at 2.7 km depth. At 3.5 km depth, the new power potential is 75% greater based on this study's temperature-at-depth maps compared to the same area within SMU's 2011 map.

Additionally, this study assesses uncertainty associated with the SRP subsurface temperature estimations based on the heat flow data set and a radiogenic heat production model. Because heat flow data vary in abundance, spatial/depth distribution, and quality, an uncertainty assessment is necessary to quantify the confidence of the presented results. We examined data attributes

[1] For more information, see https://ogcc.idaho.gov/data-explorer/.

(including quality, location, and fault proximity) and quantified heat flow interpolation variability. Results show that initial data processing and selection of regionally representative data are most important to reduce interpolation uncertainty. Where possible, heat flow data are limited to "B" quality values, meaning measurement error is up to 20%. Many of the new data added are bottom-hole temperature (BHT)-derived heat flow values, which are assigned a "BHT-C" quality, considered to have up to 25% measurement error. Limiting the data set to only the higher-quality values reduces the overall number of data points, but allows a higher confidence in the final results to be possible.

Data removal using a 2.5-km buffer around each fault trace is suggested to inhibit potential advective heat flux. As this study shows, wells within the buffer produce a pattern that we interpreted to indicate fluid inflow and outflow as represented in mapping with a lower and higher heat flow signature, respectively. Data removed based on a 5-km buffer is too much, such that it produces random changes in the heat flow grid. Use of fault buffers change mapped heat flow typically by less than 20%, which is equivalent to the error assigned to "B" quality data. None of the final 206 data points are removed from the heat-flow-calculating data set based on proximity to fault trace, because the percent change is within heat flow measurement error; however, these results are important to consider, particularly with future conventional geothermal exploration in the SRP because the heat flow patterns may indicate fluid flow pathways.

Additional temperature-at-depth calculation uncertainty is from the radiogenic heat production model, which follows the heat flow-radiogenic heat production (Q-A) relationship. The thickness of the radiogenic heat-producing layer is unknown, but estimated to be between 5 km and 10 km based on previous seismic studies. Model sensitivity of the radiogenic heat production model and resulting temperature-at-depth calculations are tested by varying the heat production layer thickness from 5 km to 10 km and examining temperature change at 4 km. Calculated temperatures vary by 10% (up to 27°C), although most temperature change is less than 5%. This again is less than the 20% measurement error assigned to "B" quality heat flow data and is considered a minor factor in final temperature estimates.

Examination of heat flow, radiogenic heat-producing layer thickness, and whole rock geochemistry revealed the Q-A relationship may be an oversimplification of the SRP thermal regime. Radiogenic heat production is approximately 12 to 40 mW/m² for this region, and mantle heat flux is set at 60 mW/m² for this study, following previous U.S. resource assessments. Thus, measured heat flow above 100 mW/m² is unaccounted for in the Q-A relationship and must derive from an additional heat source. This anomalous heat flux may be heat refraction, advection, additional mantle heat flux, or a combination. Many data sites along the SRP margins and in the ESRP contain anomalous heat flow, whereas the WSRP is generally lower than the 100 mW/m² cutoff. This discrepancy in the Q-A relationship for the SRP suggests that the region's geologic complexity is also evident in the thermal regime. More research needs to be done to refine the Q-A relationship in the SRP, which will ultimately lead to more refined thermal models and resource assessments of the region.

Section 1 in its entirety was submitted to the Geothermal Rising (previously the Geothermal Resources Council) Annual Meeting and was presented as a PowerPoint presentation and written paper in October 2020. The abstract contained in Section 2 was also submitted to the Geothermal

Rising Annual Meeting and was presented as a poster presentation in October 2020. The rest of Section 2 is an explanation for the work associated with the subsurface temperature uncertainty analysis. Section 3 is a summary section containing the conclusions of Sections 1 and 2 and suggested next steps associated with the results of this research.

Table of Contents

List of Figures

List of Tables

1 Shallow Geothermal Potential of the Snake River Plain

1.1 Abstract

The Snake River Plain (SRP) terrestrial heat flow and subsurface thermal regime are not well understood, but are important for assessing the local geothermal resource potential, both for conventional and for enhanced geothermal systems (EGS) development in the region. Resource evaluation for the SRP is complicated by the disparate data density, along with the known lateral advection of heat in the Eastern SRP Aquifer (ESRPA) and vertical heat transport by fluids in the bounding faults, primarily in the southwestern section. Fortunately, recent studies (e.g., the Snake River Plain Play Fairway Analysis, the Idaho FORGE site, and site-specific investigations, which included drilling within the Camas Prairie and on the Mountain Home Air Force Base near Twin Falls and in the Eastern SRP [ESRP] as part of the *HOTSPOT* Project) add both drilling and geophysical data. The SMU Geothermal Laboratory has conducted detailed studies of SRP tectonics and heat flow since the 1970s and used this knowledge as part of the EGS geothermal potential estimation for the conterminous United States in 2006 and again in 2011, calculating geothermal potential from 3.5 km to 10 km depth. Recent temperature modeling refined the calculation methodology to estimate shallow (1 km to 4 km) resource potential using an improved thermal conductivity model and incorporation of shallow groundwater flow. By incorporating the new SRP geology, geophysics, and 206 thermal data sites into the SMU thermal modeling methodology, this project updates the resource estimate for the SRP, and generates new temperature-at-depth maps for the shallow subsurface (1 km to 4 km). The project results highlight the EGS potential resource areas (≥150°C) and areas with more exploration risks based on minimal and/or low-quality data. The newest temperature modeling results suggest EGS potential is nearly five times greater in the SRP than previously estimated.

1.2 Introduction

The SRP, part of the Yellowstone Hotspot track, has been a target for geothermal energy production for nearly 50 years. Previous research studied the broader thermal regime for southern Idaho and its interactions with the hydrological regime across the SRP and more specifically the ESRPA (Blackwell 1969, 1971, 1989, 1992; Brott et al. 1976, 1978, 1981; McLing et al. 2016). Early studies collected small amounts of regional data for geothermal exploration, including areas in central Idaho near known Idaho batholith hot springs, the ESRP, Camas Prairie, Owyhee Plateau, Grandview, Rexburg/St. Anthony/Teton River, Weiser, and others (Blackwell, 1969, 1971, 1989, 1992; Brott et al. 1976, 1978, 1981). These works were a collaboration of industry exploration, fundamental research, and early-stage exploration-driven research.

Much of the shallow thermal regime is characterized by high ground flows (up to 1 km/yr in the ESRPA and artesian flow of 0 to 40+ gal/min in wells throughout the SRP) in local to regional aquifers. Consequently, geothermal energy production in the SRP will likely be realized through the utilization of EGS. This study provides insight into the thermal regime of the upper 1 km to 4 km of the SRP, with specific interest in temperatures above 150°C for future EGS exploration

and development, by utilizing the most recent temperature calculation methodology combined with reevaluation of new and old temperature data, an updated thermal conductivity model, and geologic and geophysical subsurface crustal models. This effort builds from a series of works that improved the methodology and tools for broad-scale heat flow and temperature-at-depth mapping, which produce higher-resolution results by estimating heat flow and temperatures for every data point location with detailed temperature and thermal conductivity models (Blackwell et al. 2006, 2011b; Stutz et al. 2012; Frone et al. 2015; Jordan et al. 2016; Smith 2016; Smith and Horowitz 2016). As part of this project, the model steps do not change; rather, the data input is refined based on availability to data that represent the deep regional thermal regime.

The most recent geothermal projects in the SRP include the SRP Play Fairway Analysis (Shervais et al. 2020), the Idaho Frontier Observatory for Research in Geothermal Energy (FORGE) project (McCurry et al. 2016; Podgorney et al. 2016), and the *HOTSPOT* Drilling Project (Shervais et al. 2012). The recent studies add geological and geophysical understanding and provide opportunities for comparison in the Camas Prairie (Glen et al. 2017, 2018; Shervais et al. 2020), the Mountain Home (Lachmar et al. 2019), and in the ESRP at the 2010-drilled Kimama well. This project increases the knowledge of the deeper thermal regime through the addition of deep (700–4,000 m) oil and gas wells, new geothermal wells, and reassessment of heat flow data (well temperature gradients, thermal conductivities based on rock cores or lithology, and radiogenic heat production of actual samples and predicted values). Other relevant data are also examined, including Quaternary fault lines, volcanic formation ages and locations, geological cross sections, and review of previous results from gravity and magnetic maps that define aquifer thickness and interpreted lithologies (Whitehead 1992; Lindholm 1996). Improvements on past research include the updated thermal conductivity model and increased mitigation of error from groundwater flow in the thermal model (Blackwell 1989; Blackwell et al. 1992).

The geothermal resource is defined here for the first time by its temperature component between 1 km and 4 km, utilizing additional temperature data, thermal conductivity, lithology, and crustal structure studies combined with the most recent heat flow and temperature-at-depth calculation methodology. The additional data increase the resolution and variability of temperature estimates, and the new temperature estimates make it possible to examine where EGS opportunities may occur in the region. The resulting temperature-at-depth maps and updated resource estimate for each 1 km depth thickness below the SRP highlight areas with the greatest EGS potential and areas with the highest risk associated with sparse or low-quality data.

1.3 Snake River Plain Geology

The SRP is a physiographic region defined by the arcuate topographic low visible on elevation maps that formed in response to the interaction between the North American Plate and the Yellowstone Hotspot. The SRP can be divided into three areas: the Western SRP (WSRP), Central SRP (CSRP), and the Eastern SRP (ESRP) (see Figure 1). Although they are different, all three subregions are thought to be related to the Yellowstone Hotspot. The detailed geologic history of the SRP is described by Wood and Clemens (2002), Shervais et al. (2002), and Pierce and Morgan (2009). The CSRP and ESRP can be described broadly as a series of young, small basaltic eruptions underlain by older felsic calderas. In this way the SRP differs from the Columbia River Basalts to the west, which are thick and widespread flows. This difference is

visible in temperature logs, with Columbia River Basalts exhibiting a stair-stepping pattern associated with confined aquifers at the base and top of basalt flows that become connected in open-hole sections of a well (Blackwell et al. 1990; Frone et al. 2015). In contrast, temperature logs within SRP basalts show a large isothermal zone throughout the section because the thin basalt flows do not confine aquifer flow. The WSRP formed as a rift-style basin through lithospheric weakening from the passing Yellowstone Hotspot (Wood and Clemens 2002). Lacustrine sediment packages are interbedded between basalt flows in the WSRP (Wood and Clemens 2002). Various exploratory drilling penetrates felsic rock on the margins of the WSRP, but the deepest wells in the center of the basin do not intersect felsic rocks.

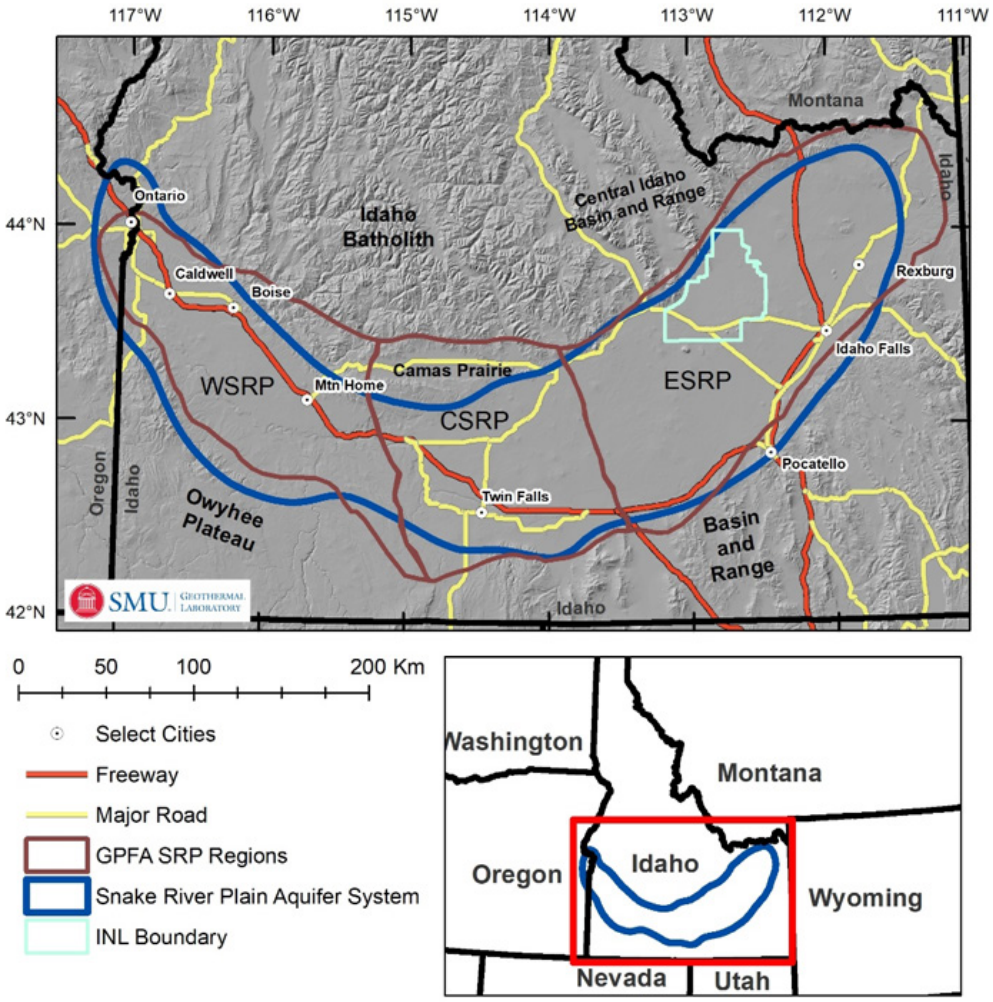

Figure 1. The SRP region of Idaho and Eastern Oregon. The study area is defined by the U.S. Geological Survey (USGS) as the SRP Aquifer System, the blue outline (U.S. Geological Survey, 2015). The recent Geothermal Play Fairway Analysis (GPFA) defined the SRP slightly differently, following the brown outline.

Note that INL stands for Idaho National Laboratory.

Studies in the Cascade Range, Columbia Plateau, and SRP clearly show that basalt permeability relates to degree of alteration (Bargar and Keith 1999; McLing et al. 2016; Frone et al. 2015; Lachmar et al. 2017). High-temperature alteration or prolonged low-temperature groundwater flow that leads to mineral precipitation reduces permeability in basalt pore space and fracture zones, which inhibits groundwater flow and establishes a conductive thermal regime. We observe evidence for these same phenomena in the ESRP (Whitehead 1992; Lindholm 1996), and they may exist at other sites, including the Kimama drill hole in the ESRP (Lachmar et al. 2017) and in drilling at Newberry Caldera (Bargar and Keith 1999). Hence, in the SRP basalt aquifer, the thermal regime tends to be isothermal throughout the thickness of the aquifer from high flow rates through the connected pore and fracture permeability (see temperature log examples in McLing et al. 2016), whereas in the Cascade Range and Columbia Plateau, heat flow may be conductive over much of a system of confined aquifers. The domination of lateral and vertical convective flow in the SRP in the top 100+ m means that only wells that completely penetrate these flow zones may give useful thermal information.

Faults were also used in the SRP Geothermal Play Fairway Analysis (GPFA) as a potential indicator for geothermal power potential, specifically as an indicator for higher permeability (Shervais et al. 2015, 2020). There are two primary regional fault trends that crosscut the SRP. The WSRP has a WNW-trending fault system associated with formation of the sag and graben WSRP basin. This fault trend is young, Miocene to Quaternary aged, and bounds the northern and southern boundaries of the WSRP (Ludington et al. 2005; Machette et al. 2003; Wood and Clemens 2002). These faults are high angle, with fault motion mostly normal and some minor oblique-to-strike-slip movement. Previous work highlights the WNW fault trend as a primary permeability target for geothermal exploration because of the age, density, and slip tendency of these faults (DeAngelo et al. 2016; Shervais et al. 2020). The second regional fault trend strikes NNW to N, encompasses much of the area surrounding the SRP, and is hypothesized to underlie the ESRP (Rodgers et al. 2002). This fault group is primarily older, but contains some Quaternary faults, mostly north and southeast of the SRP. These faults are thought to underlie and account for extension of the ESRP as continuations of the range bounding faults visible both north and south of the ESRP (Rodgers et al. 2002). These faults could alternatively form through cooling-related subsidence (Pierce and Morgan 2009). In this study, the faults of most interest are Quaternary-aged faults because the recent fault movement is hypothesized to have more potential for fluid flow, and with fluid flow would contain advective thermal signatures not representative of the regional conductive thermal regime.

1.4 Method, Model Inputs, and Data

The thermal model used here is the simplified steady-state one-dimensional heat diffusion equation with additional radiogenic heat production to produce site-specific heat flow and temperature-at-depth calculations. The methodology uses an input of a thermal conductivity model and geothermal gradient data for each site to first calculate terrestrial heat flow, which then becomes the foundation to calculate the deeper temperatures-at-depth. Next, the new heat flow, thermal conductivity model, and assumed basement properties become inputs to calculate temperature to a given depth (Smith 2016; Smith and Horowitz 2016). We reevaluated and filtered available well data to remove advection-influenced temperature data and incorporated geological and geophysical data to refine sediment thickness and stratigraphy for the site-specific thermal conductivity models. New geophysical studies are also used to define the thickness of

the upper crust for radiogenic heat production. These changes improve the accuracy and resolution of the resulting temperature estimates and geothermal resource potential.

1.4.1 Model Parameters

For this study, we incorporate surface temperature, temperature logs, bottom-hole temperature (BHT), lithology logs, thermal conductivity measurements, mapped aquifer temperature and thickness, upper crust thickness estimates from seismic studies, and previous regional cross sections to generate a new heat flow map gridded at 3' by 3' spacing. Data are examined so that the final maps are representative of the deep (>1.5 km), conductive, regional thermal regime. Specific input data utilized for the heat flow and temperature-at-depth calculation and how these differ from previous SRP resource estimations are discussed next.

1.4.1.1 Site Temperature and Heat Flow Data

Temperature data from equilibrium temperature logs and BHTs are utilized to calculate geothermal gradient for heat flow calculations. New criteria are applied based on the well temperature source being either an equilibrium temperature-depth log or a BHT measurement (Table 1) and then filtered based on maximum depth of temperature (Table 2). Temperature log data shallower than 125 m are eliminated to remove potential near-surface influences not representative of the deeper thermal regime. BHT measurements shallower than 600 m are eliminated to minimize drilling disturbances following methods in Blackwell et al. (2010). A second-level site-by-site filtering of the data removed additional sites with temperature measurements displaying localized temperature phenomena (i.e., an isothermal section or temperature overturn) that do not reflect the deeper (1 km to 4 km) subsurface thermal regime. Resulting available data are used to calculate the site geothermal gradient. Geothermal gradient is calculated from the deepest conductive zone for equilibrium temperature logs, or from surface to depth of BHT for BHT-only wells, utilizing near-surface water temperature from Gass (1982) as the surface temperature. With all these filtering criteria incorporated, the southern Idaho data set is reduced from 926 to 206 data points (Figure 2). New temperature data include 74 BHT measurements and 2 temperature-depth logs, which is approximately 40% of the temperature data. The 206-point temperature data set improves upon previous work in that the temperature gradients are all interpreted to represent the deep regional thermal regime.

Table 1. Temperature Data Selection Criteria

Temperature Measurement Type	Specific Criteria for Well Site Inclusion in Study
Temperature-Depth Log	Deeper than 125 m Conductive, linear gradient if at bottom of well log (convection/isothermal section okay if not deepest section) Bottom depth not within a known geothermal system well (e.g., Boise, Camas Prairie—Magic Reservoir, Rexburg)
Bottom-Hole Temperature (BHT)	Deeper than or equal to 600 m BHT value as compared to other surrounding data indicates a linear gradient

Table 2. Well Temperature Data Distribution by Depth

Depth	Number of Sites	Number of Sites Used	Percentage of Original Data
Near Surface (<125 m)	490	0	0%
Shallow (125–600 m)	245	142	26%
Medium (>600 m)	84	50	9%
Deep (>1,000 m)	114	57	12%

Compilation of the terrestrial heat flow data includes: (1) the SMU Geothermal Laboratory heat flow data on the National Geothermal Data System, (2) the related SMU temperature-depth well logs for southern Idaho and eastern Oregon, (3) the Idaho Geologic Survey borehole temperature content-model data set, (4) new temperature-depth well logs associated with the *HOTSPOT* Project (Utah State University 2014a, 2014b, 2014c) and (5) Idaho oil and gas exploration well lithology and temperature data collected for this project from 24 Idaho sites drilled after 2007 (sites newer than current upload in the Idaho Geologic Survey data collection for the National Geothermal Data System (Figure 2)). The Oregon Department of Geology and Mineral Industries borehole temperature content-model and online geothermal well database (GTILO-2_Geothermalwell_database.xls) were also examined for additional new data.

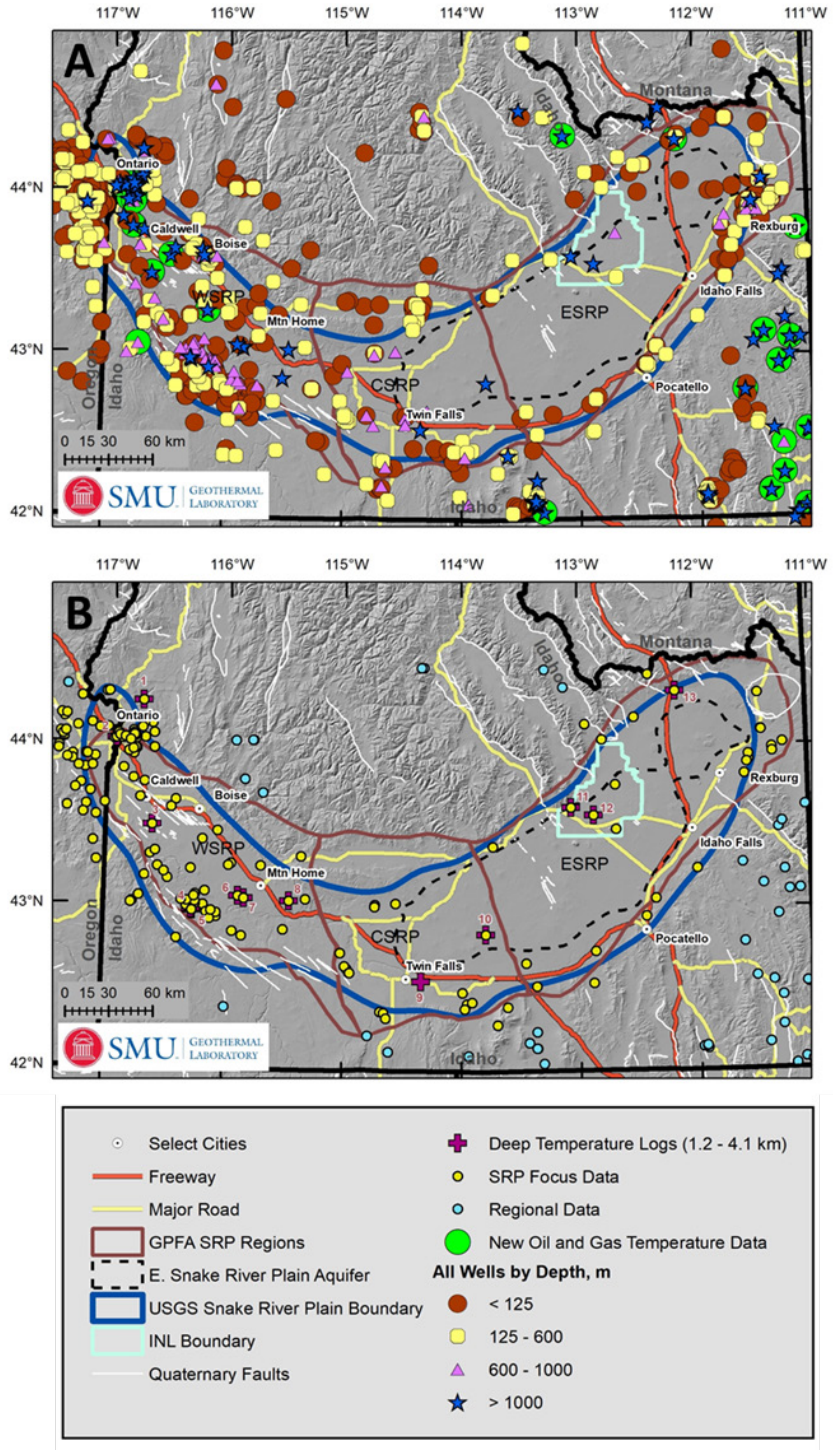

Figure 2. Data location plots.

(A) Temperature points plotted by depth of bottom temperature measurement. Note that there are more than 926 points on this figure because of wells with multiple temperature values. At locations with multiple heat flow values, the value with the highest confidence is used for further calculations.

(B) Data in southern Idaho that pass all data filtering criteria. These data record the deep thermal regime and are used for temperature-at-depth and resource potential calculations. Data within 20 km of the USGS SRP boundary are the yellow data, and data outside this 20 km buffer are the light blue dots. The regional data are included in interpolation to minimize boundary interpretation errors within the SRP.

1.4.1.2 Geology, Lithology, and the Thermal Conductivity Model

A thermal conductivity model is constructed for each site and used in calculating the terrestrial heat flow and extrapolating temperature to given depths. The generalized stratigraphic column total thickness is set equal to the depth to basement, and individual stratigraphic bed thicknesses are uniformly scaled to fit the new total column thickness, while conserving percent thickness of each formation. This site-specific stratigraphic column, with estimated thermal conductivity of each stratigraphy intersected, is then used to calculate a depth and thickness weighted thermal conductivity, which is used for heat flow and/or temperature-at-depth calculations (Blackwell et al. 2010; Smith and Horowitz 2016). Each site is assigned a site average value using this process. Only measured thermal conductivities within the SRP are utilized for constructing the thermal conductivity model. Although only using SRP measured values increases potential error because of a low sample size, this method is preferred because measured values are coming directly from the study area and are therefore more representative.

Sedimentary rock thermal conductivity is assigned based on the site's sedimentary rock types and related values from WSRP wells ORE-IDA 1, VALE 47-10, and Anschutz (Brott et al. 1976; National Geothermal Data System 2014), and thermal conductivity for the basalt and rhyolitic rocks are assigned from measured values from the closest applicable measured value (Table 3) (Blackwell 1989, 1992; Shervais et al. 2012, 2013; Lachmar et al. 2017, 2019). New measurements for basalt and rhyolite come from the *HOTSPOT* wells (Shervais et al. 2012; Lachmar et al. 2017, 2019). A thermal conductivity model is produced using measured values. This model is variable but generally decreases with increasing depth, based on the nearest equivalent depth measured thermal conductivity value. This decreasing thermal conductivity with increasing depth matches the Frone et al. (2015) thermal conductivity model that also decreased with increasing depth that used a thermal conductivity – temperature relationship. This study improves the thermal conductivity portion of heat flow calculations for the SRP by being the first to incorporate the site-specific depth and stratigraphy-correlated thermal conductivity models as opposed to a single estimated thermal conductivity based on drilling reports or cuttings piles (Blackwell 1989).

Compilation of the lithology data included the Idaho lithology interval content model uploaded to the National Geothermal Data System (Idaho Geologic Survey 2013); individual oil and gas, geothermal, and water wells deeper than 1,000 ft (305 m) from Idaho and Oregon; well logs from the Idaho National Laboratory (INL) FORGE project (Podgorney et al. 2016); and new lithology from the three *HOTSPOT* drilling project wells (Shervais et al. 2012, 2013) (see Figure 3). Wells are manually examined and used to construct generalized lithology sections for the WSRP, CSRP, and ESRP with estimated variability within the thickness of a given lithology section (see Final Report Appendices in Batir et al. 2020b). Aquifer thickness was estimated using electrical resistivity and is interpreted as the depth to the hydrothermally altered basalt and/or clay-filled low-porosity section (Whitehead 1992; Lindholm 1996). The lithology within the ESRPA was interpreted as unaltered basalt.

Table 3. Assigned Thermal Conductivities Based on Rock Type

Volcanic Rocks		Sedimentary Rocks	
Rock Type	**Volcanic Thermal Conductivity, $Wm^{-1}K^{-1}$**	**Rock Type**	**Sediment Thermal Conductivity, $Wm^{-1}K^{-1}$**
Rhyolite	1.75	Shale	1.2
Basalt	1.3–2.0	Sandstone	2.0
General Volcanics*	1.4–1.5	Interbedded Sandstone/Shale	1.9
Interbedded Basalt/ Shale	1.4–1.6	General Sedimentary	1.7–1.9
Interbedded Basalt/ Sediments	1.5		
Interbedded Rhyolite/ Basalt/Sediments	1.7		
Basement Conductivity (Average of Felsic Rocks)		2.3	

*General volcanics is assigned when original lithology logs did not indicate details on the thickness or percentages of respective volcanics in a section, providing no quantitative way to calculate a percent weighted thermal conductivity.

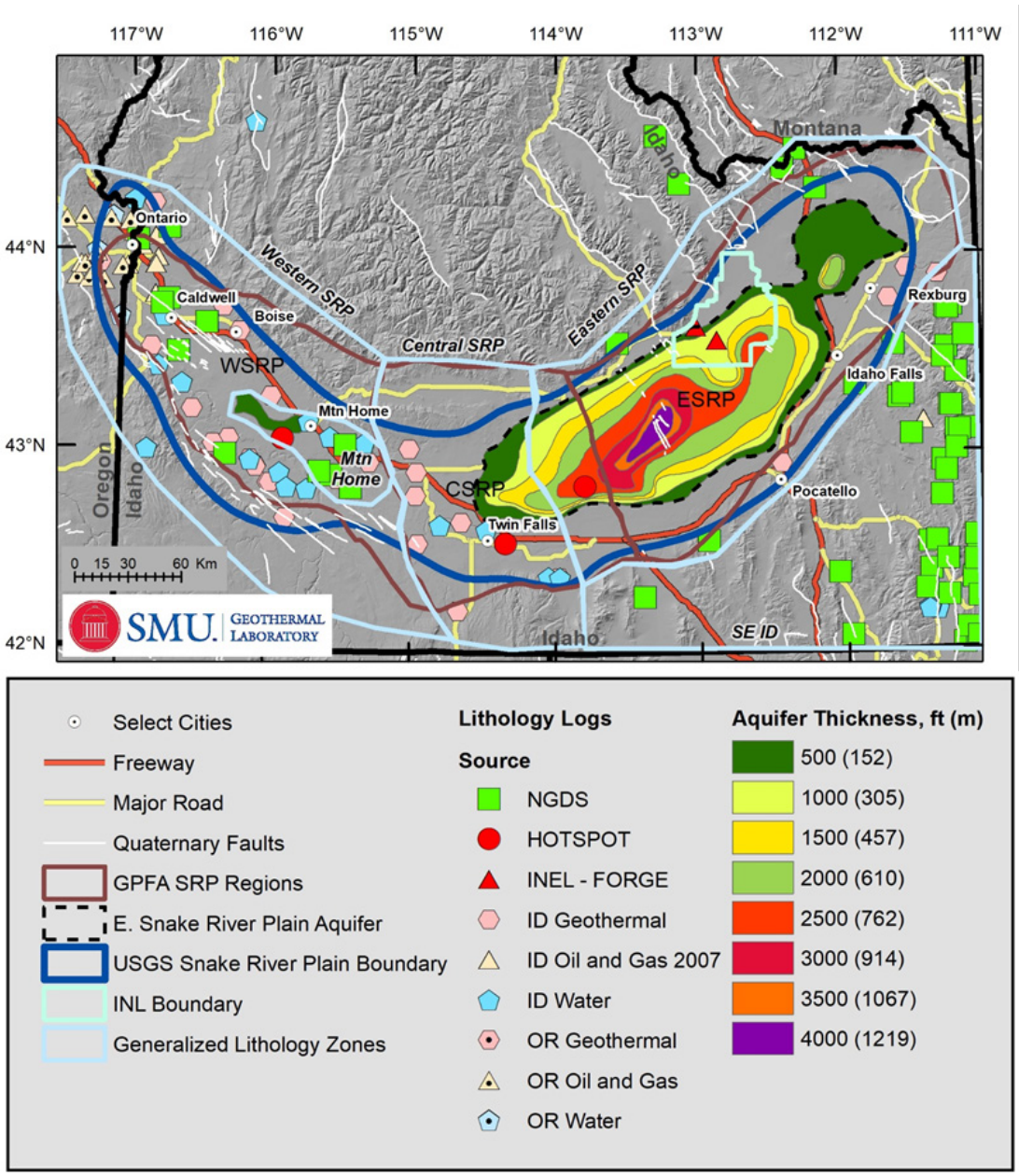

Figure 3. Data used to produce the five generalized thermal conductivity models for the SRP. Thermal conductivity model areas include: WSRP, Mountain Home, CSRP, ESRP, and SE ID, which is the area southeast of the SRP. The ESRPA thickness is utilized to estimate basalt thickness and as a temperature-depth input. The lithology columns are available in the related Final Report Appendices of Batir et al. (2020b).

1.4.1.3 Basement Parameters and Radiogenic Heat Production Model

In addition to the heat flow value and thermal conductivity model at each point, the temperature-at-depth calculation requires inputs for basement thermal conductivity, mantle heat flow (Q_m), and thickness of the radiogenic heat-producing layer (*b*) (attributed to the felsic upper crust). Inputting those values provides an estimate of the radiogenic heat production (A) contribution to the measured terrestrial heat flow (Q) (Smith 2016; Smith and Horowitz 2016). Basement thermal conductivity is assigned 2.3 W/m*K as the average of felsic rocks within the SRP (Brott et al. 1976; Blackwell 1989, 1992; SMU unpublished Kimberly research), and Q_m is set to 60 mW/m² (Roy et al. 1968). The *b* value is assigned based on sediment thickness. If sediment thickness is less than 3 km, *b* is set to 7.5 km; if sediment thickness is greater than 3 km, *b* is calculated as 10.5 km – sediment thickness. This *b* assignment incorporates new upper crust thickness estimates beneath the SRP (Hill and Pakiser 1967; Sparlin 1981; Harper 2018) and uses the *b* calculation methodology from Blackwell et al. (2007 and 2010), Smith (2016), and Smith and Horowitz (2016). The A value is calculated at each site to satisfy the Q-A relationship described by Roy et al. (1968) and Lachenbruch (1968). This calculation assumes that all other inputs into the model (Q, Q_m, and *b*) are correct, which then calculates an A value to force the Q-A relationship to be true. This heat production model improves the SRP thermal regime modeling by utilizing the recent work of Harper (2018) to redefine the *b* layer thickness, and also calculates site-specific A values so that the Q-A relationship is satisfied at all data locations.

1.4.2 Data Density, Contouring Control, and Gridding

Heat flow, as the primary data source, and subsequently temperature-at-depth data sites define the data density and appropriate grid size for mapping. The accuracy of the heat flow and temperature-at-depth maps is directly related to the density of the data and the geologic/ geophysical constraints in the model for areas without any data. Areas in the ESRP with few or no data points incorporate the aquifer depth contours to aid in defining depth to the conductive thermal regime as a way to increase the accuracy of mapping this region that has low data density.

The heat flow map is gridded in ArcGIS using Spline with a smoothing factor of 1. Gridding is performed at a more refined grid (3’ latitude/longitude) than past analysis, allowing for more inclusion of site data values. Data density is still low for the ESRP, but new data in the WSRP have increased data density, and now most of the WSRP portion of the heat flow map contains at least one data point within any 15-km radius circle (4). This heat flow map of the SRP overall has less data, yet by removal of near-surface data and temperature logs with fluid flow, the results are more representative of the deep thermal regime for geothermal resource exploration.

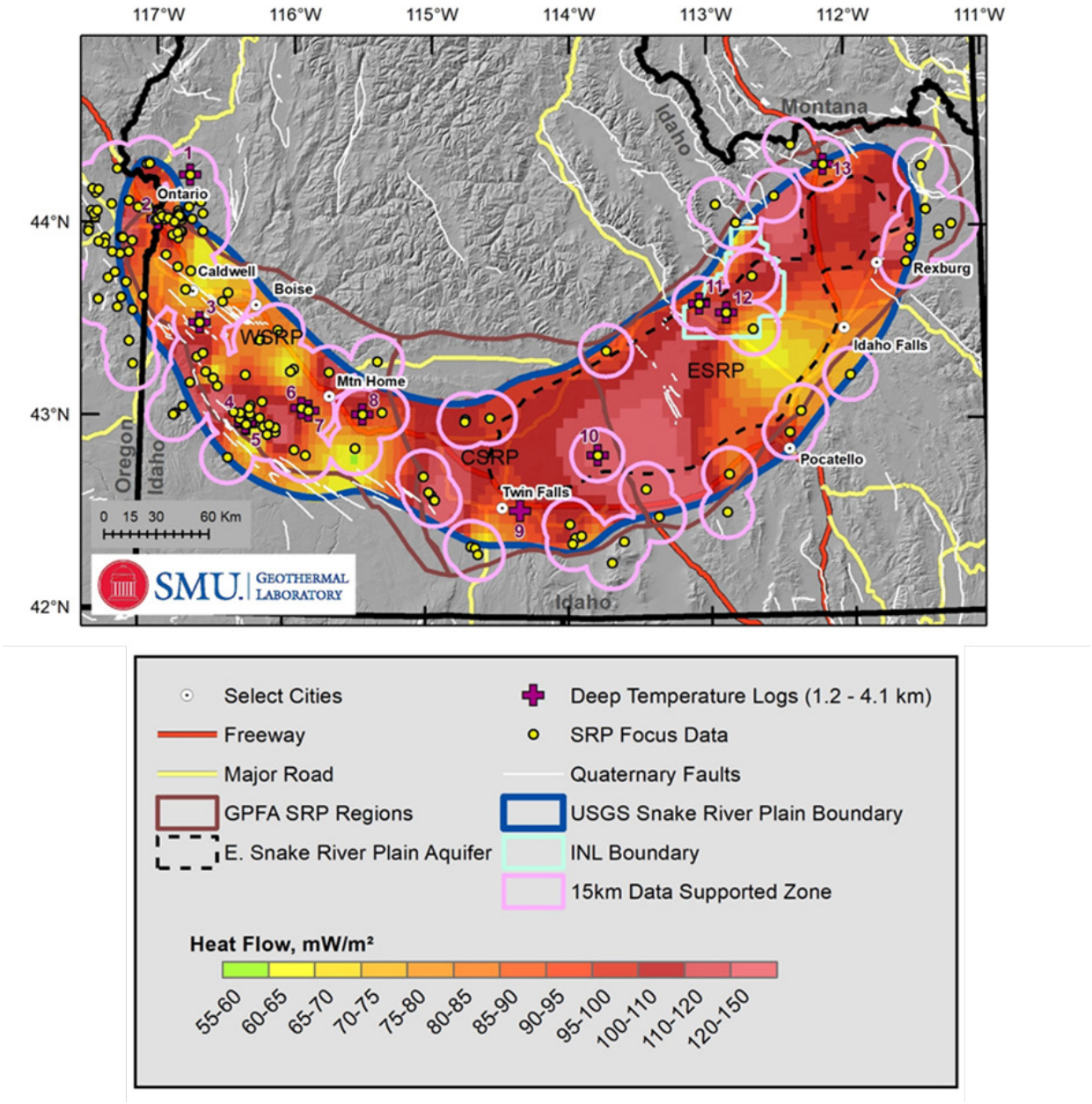

Figure 4. Terrestrial heat flow and data coverage map. Areas within the light pink outline have a minimum of one data point within a 15-km radius. Much of the WSRP is data supported, whereas much of the CSRP and ESRP have low data coverage. Deep temperature logs are displayed, showing where there are direct temperature observations to modeled depths.

Temperature logs correlate to numbers in all figures as follows: 1 = RDH-CHA #1; 2 = ORE-IDA #1; 3 = Upper Deer Flat #11-19; 4 = Federal #60-13; 5 = Lawrence D. #1; 6 = MTH #2B; 7 = Mt. Home AFB #1; 8 = Bostic #1-A; 9 = Kimberly (KMB); 10 = Kimama (KMA); 11 = INEL-GTL1; 12 = INEL-WO2; 13 = Hagenbarth #22-25.

1.5 Results

Surface heat flow values, temperature-at-depth calculations, and a percent difference of the modeled versus observed temperatures are presented as maps for the SRP region along with the regional data (Figure 5–Figure 10). The heat flow map is based on the newest heat flow determination for the SRP, which utilizes the 206 data points considered to be representative of the regional thermal regime. Based on the heat flow, the thermal modeling outputs the resulting temperatures, which are mapped in 25°C increments from 100°C to 250°C+ for consistency in mapping the EGS resource potential. The current EGS electricity production potential values are calculated with a temperature cutoff of 150°C, yet temperature maps display temperatures to 100°C for future reference as improvements are made and lower temperatures can be economically utilized for power production. Additionally, the high-temperature contouring is limited to 250°C+ to limit gridding in areas of sparse data, and to not overemphasize regions of high extrapolated temperatures. The equilibrium temperature measurement in the Bostic 1A well is 188°C at 2.7 km with a gradient of 66°C/km, which extrapolates to 274°C at 4 km, agreeing with model temperature estimates (Batir et al. 2020b, see Appendix for site details). Although these extrapolated temperatures agree with observed temperatures where available at shallower depths, all extrapolated temperatures are inherently higher risk because of the lack of direct observation.

In general, the ESRP has higher heat flow than the WSRP, although this comparison is biased by data distribution. There are approximately 90 data sites within the WSRP, 16 in the CSRP, and 17 in the ESRP. Wells in the CSRP and ESRP are primarily located along the SRP margins, whereas the WSRP contains a more even distribution of data between the margins and SRP central axis. Temperature distribution is variable. The CSRP and WSRP contain a variable temperature distribution tied to spatial data location. The ESRP contains primarily higher-temperature estimates except for a large low-temperature region from the southeast border of INL property, north to Rexburg, and southeast to approximately 25 km northeast of Pocatello. This low is driven by one lower heat flow point and the presence of the ESRPA. Similarly, the high-temperature region in the western part of the ESRP is interpolated from the Kimama well. Although these are high-quality data and show a conductive, linear gradient below the ESRPA, interpolation for this large area is controlled by a low number of data points and needs further study.

We assess potential uncertainty in the temperature maps by comparing measured BHT to the modeled BHT for wells greater than 750 m as a BHT percent difference map (Figure 10). The measured BHT is subtracted from the modeled BHT and calculated as a percentage on the measured BHT to determine a percent error in calculating measured BHT. A negative percent error means the modeled temperature is less than the measured, and the thermal model is underpredicting the measured temperature value. A positive percent error means modeled temperature is greater than the measured, and the thermal model is overpredicting the measured temperature value. Most wells have a modeled temperature within 10% of the measured temperature. Because most of the deep temperature measurements are oil and gas BHT measurements, 10% is within the error of temperature measurement and shows that the modeled temperatures are in good agreement with measured temperature values.

There are several underpredicted temperature values in the SRP. One well near the Vale geothermal anomaly in the far western WSRP is underpredicted by 20% to 30%. This area is a known geothermal anomaly, although temperature logs from this anomaly were included in mapping because they display a conductive, linear gradient. Similarly, wells near the Rexburg geothermal anomaly in the ESRP and wells near Mountain Home are underpredicted by 10% to 20%. The Rexburg area is another known geothermal anomaly, and the Mountain Home region contains a potential geothermal resource (Lachmar et al. 2019). These underprediction areas suggest the temperature model is best suited for regional thermal mapping and underpredicts known geothermal resource areas. This is expected because the local thermal regime of a geothermal anomaly will be hotter than the background thermal regime, which is preferentially predicted by the temperature modeling. We consider this a conservative resource estimation model because deep temperature estimates that are incorrectly predicted are less than the measured temperature. This model, therefore, errors on the side of underprediction as opposed to overprediction of potential resource.

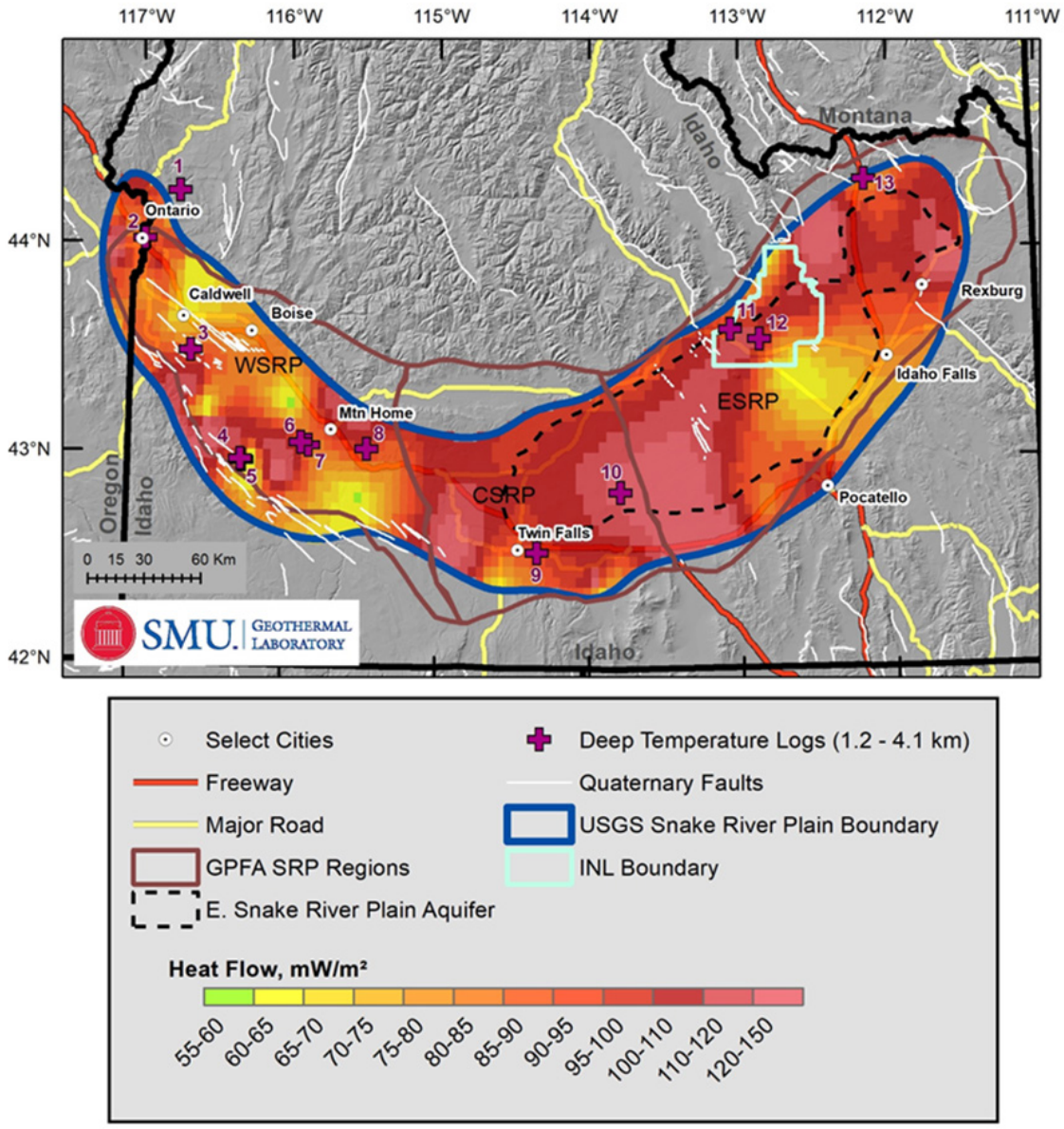

Figure 5. Terrestrial heat flow of the SRP. There is generally high heat flow in the range of 90–150 mW/m², with some select zones of heat flow in the 55–60 mW/m² range.

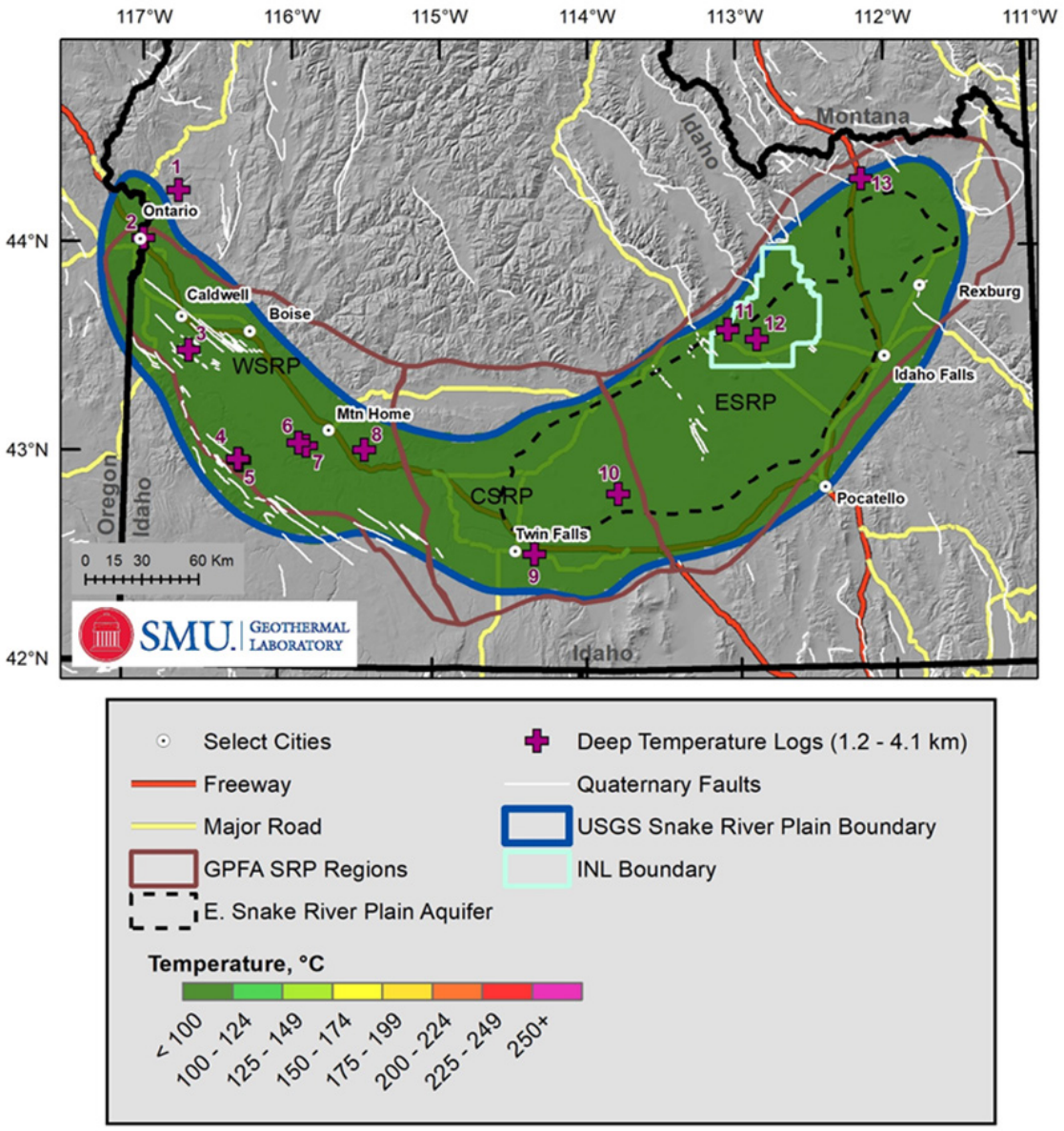

Figure 6. Estimated temperature at 1 km depth. The entire SRP region is below 100°C at this depth, which is below the EGS electricity production lower limit of 150°C. While the temperatures preclude EGS development, there is potential for conventional uses of lower-temperature geothermal fluids (e.g., direct use of the thermal resource for heating applications).

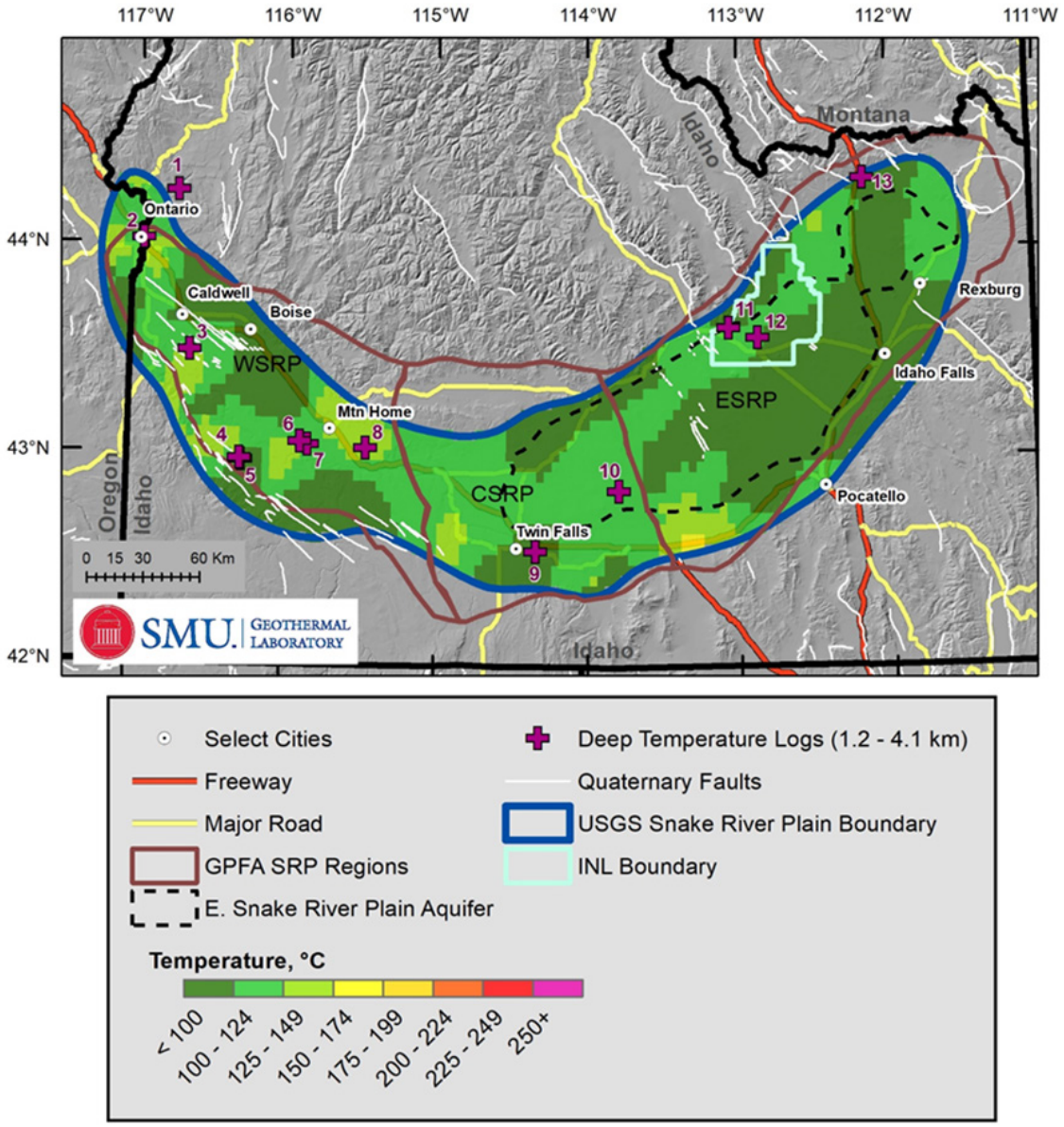

Figure 7. Estimated temperature at 2 km depth. Temperatures are generally higher than at 1 km depth, although some zones are still less than 100°C. Areas with temperature lower than 100°C roughly align with surface outcrops of volcanic rocks and a resulting thin layer of sediment cover.

There are several areas at 2 km depth with estimated temperatures of 150°C or greater (yellow squares). Those are designated as areas with EGS potential. Most of these zones are interpolations and not directly measured temperatures. Any area not directly tied to measured temperatures should be interpreted as requiring additional information and drilling to confirm resources in high-temperature areas and eliminating areas too cold to be a resource.

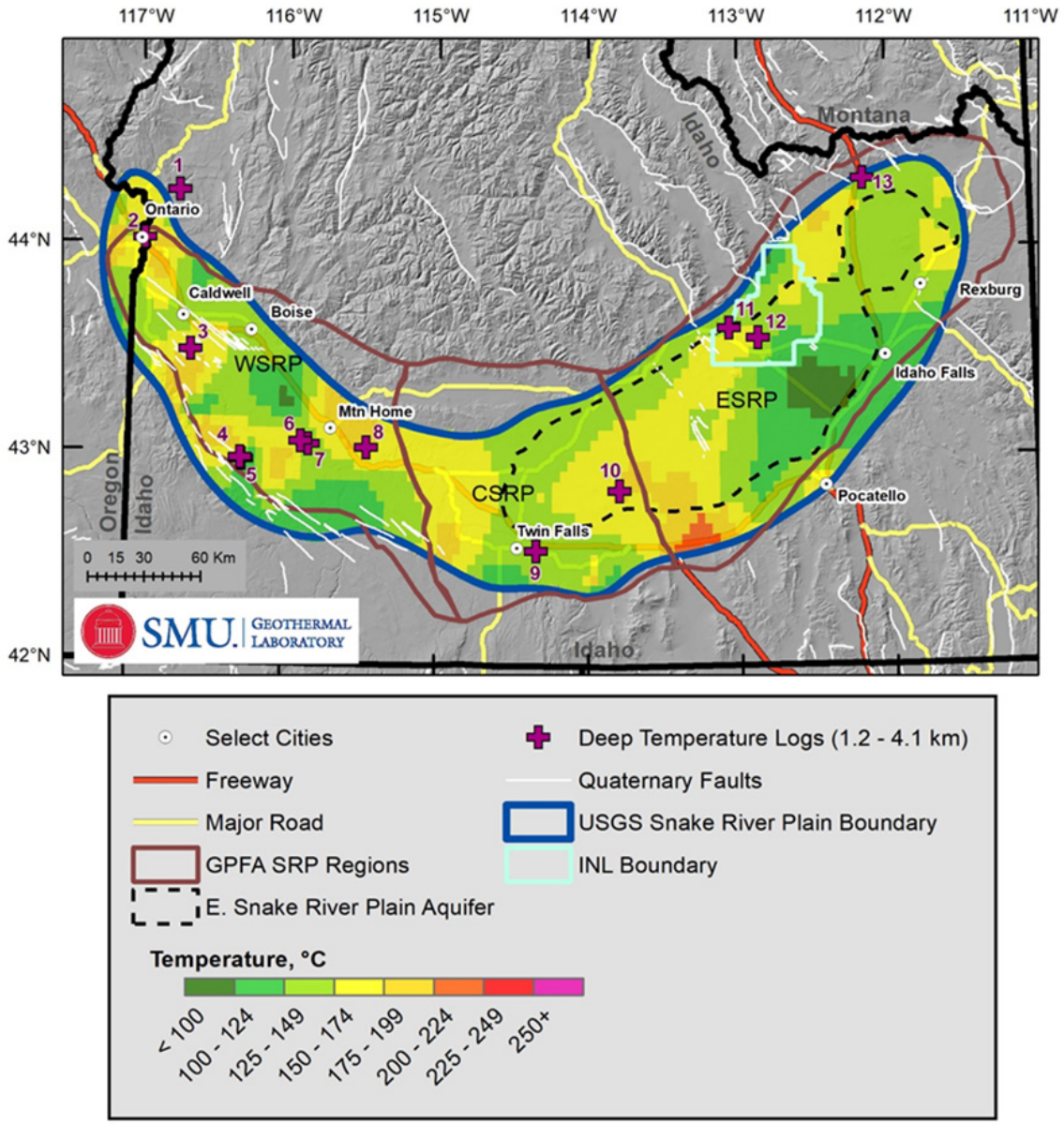

Figure 8. Estimated temperature at 3 km depth. Similar patterns of temperature are visible as seen in the 2 km temperature map. The same higher-temperature areas at 2 km are locations calculated at this depth to be greater than or near 200°C (orange to pink colors). These high-temperature values may be the result of surface heat flow measurements associated with a shallow (upper 500 to 1,000 m) thermal anomaly.

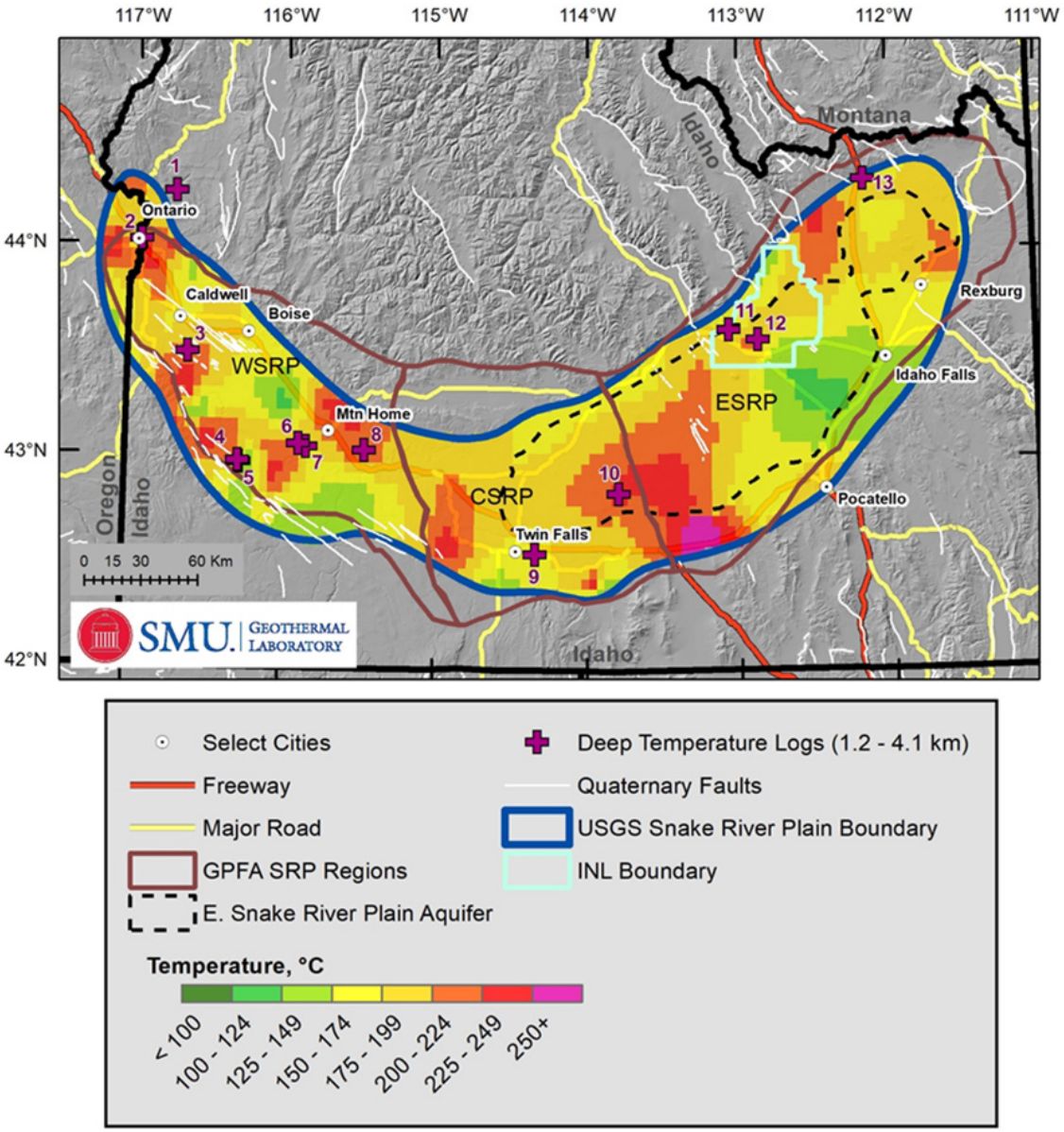

Figure 9. Estimated temperature at 4 km depth. Large sections of the SRP are predicted to be at a temperature capable of producing electricity at 4 km depth. High-temperature regions at this depth require further examination through drilling and/or additional geophysical/geochemical work.

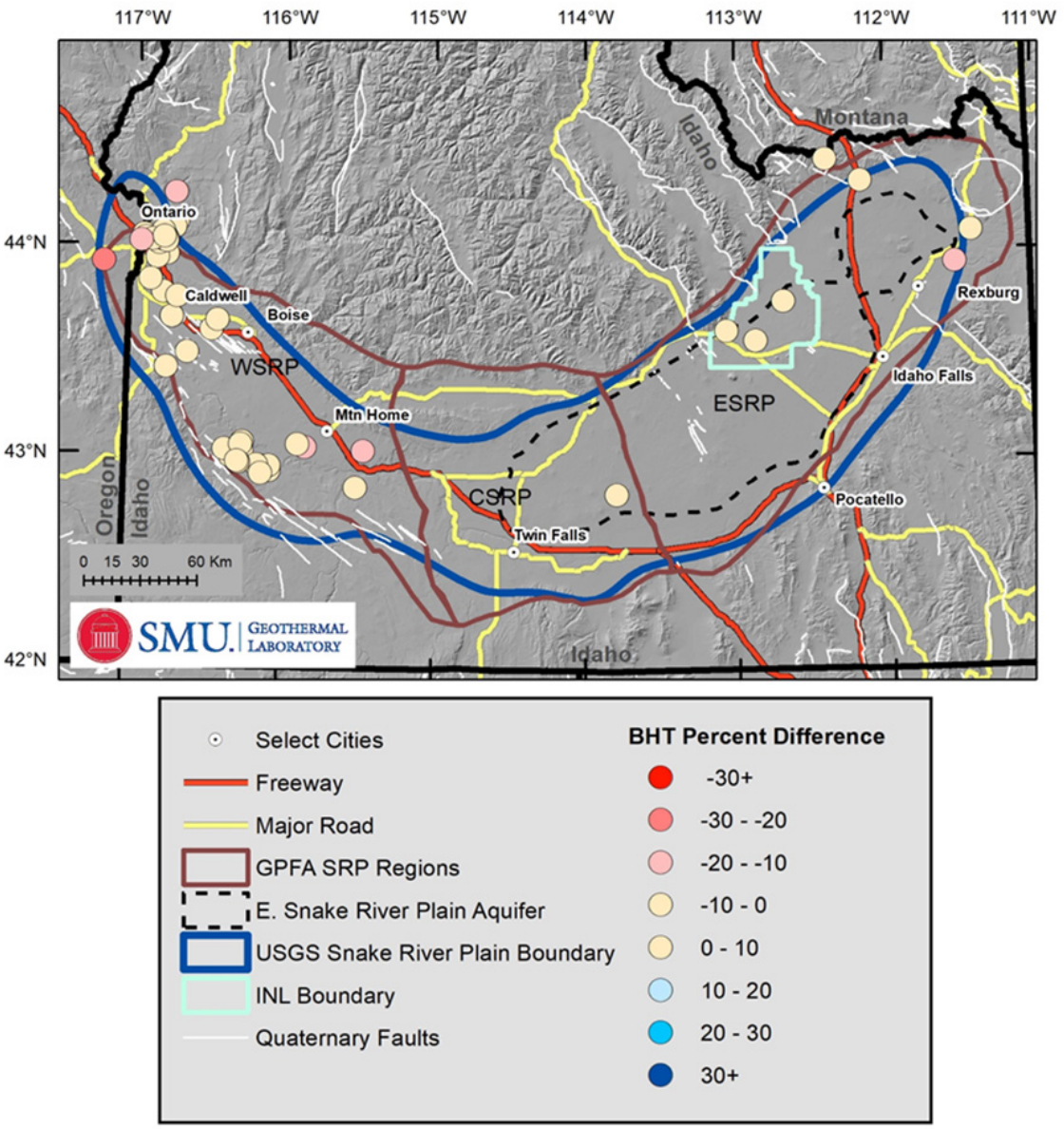

Figure 10. Percent difference of calculated BHT minus observed BHT at the measured temperature depth. The model underpredicts observed temperature where there are negative percent difference values and overpredicts temperature where there are positive percent difference values.

1.5.1 Western Snake River Plain

Many of the new data are BHT-derived heat flow in the WSRP. The new data generally agree with previous heat flow and temperature estimations but contain additional variability because of the higher number of values (Figure 11). The average for new WSRP heat flow values is lower than previous studies: 88 ±19 mW/m² for this study compared to 99 ±4 mW/m² in Blackwell (1989). The lower heat flow average for new data is expected because new data are focused in the central, deeper sedimentary sections of the WSRP. Blackwell (1989) observed the same lower heat flow trend from shallow temperature log data collected in the 1970s and 1980s throughout the central WSRP. There are several high-temperature zones within the WSRP. Most

of these are along the margins, similar to previous studies and additional high-temperature anomalies along the central axis of the WSRP running between Mountain Home and Caldwell. Additional data east of Ontario supports the elevated geothermal gradient and heat flow first seen in the ORE-IDA No. 1 well. One variation between the new map and previous works is the heat flow and temperature estimation along the southwestern margin, near the Owyhee Plateau. New data show one high-heat flow region in between low-heat flow regions. These three zones are within the Quaternary SRP bounding fault zone (Figure 11). Although all data used to create this map are considered representative of the regional thermal regime, this complex thermal pattern may be the result of regional fluid flow that is not easily detected within BHT-derived heat flow values.

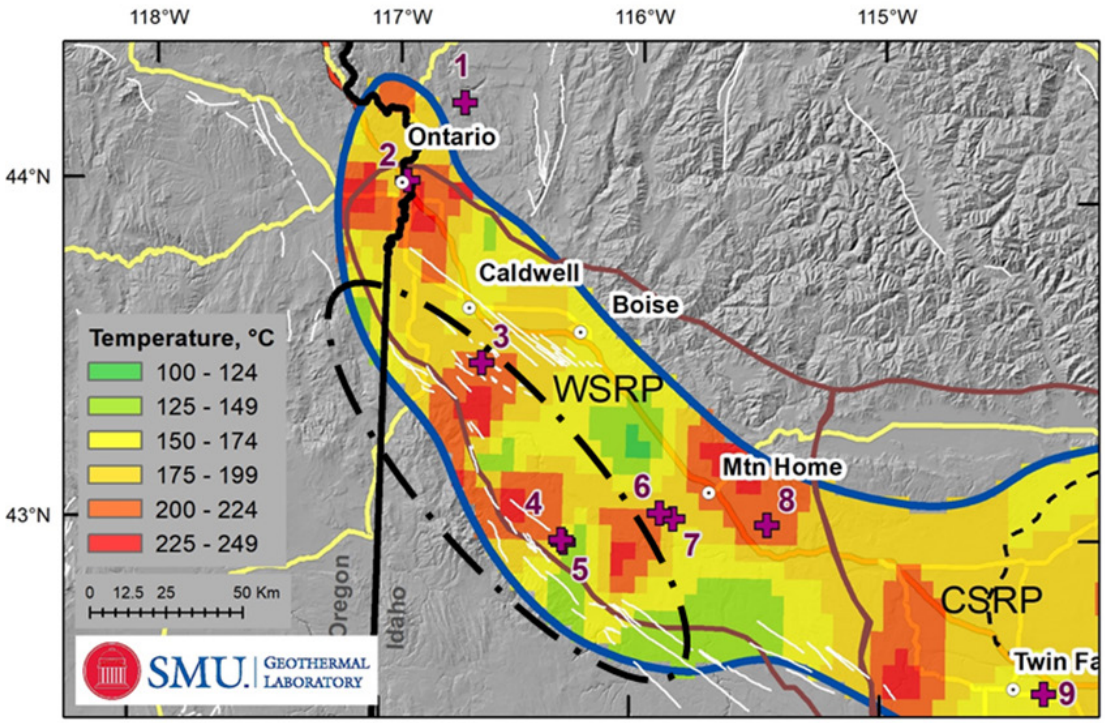

Figure 11. Temperature at 4 km depth in the WSRP. The complex thermal signature, potentially related to fluid flow along faults, is highlighted along the southern margin (black dashed oval).

1.5.2 Estimated Electrical Potential

Electrical potential is estimated following the same procedure used by Frone et al. (2015) (Table 4), which is from Augustine (2011). The calculation is for volume of 1 km centered at each kilometer depth interval. Non-development areas defined by the National Renewable Energy Laboratory are removed. Our new estimates suggest there are ~44,000 MW_e of EGS electrical potential within the SRP to 4 km. This is assuming a 20% recovery factor. Many of the energy estimates are from the 3 km and 4 km depths and in the 150°–225°C range, although there are some estimates of electrical potential in the 2-km depth range. The 2-km high resource potential region near Mountain Home is based on well control with temperatures of 127°–140°C and 188°C at 1,600–1,900 m and 2,712 m, respectively. The high estimated temperature at 2 km along the southern margin of the SRP, between Pocatello and Twin Falls, does not have deep

temperature control and is considered less constrained and therefore a higher risk area for exploration.

Table 4. Estimated Electrical Power Production for the SRP

Temperature Interval (°C)	MW_e per Depth (km)				Total Potential (MW_e)
	1	2	3	4	
150–175		109	10,213	7,814	18,136
175–200			2,708	12,139	14,846
200–225			281	7,725	8,006
225–250				2,434	2,434
250–275				371	371
275–300					
Totals	0	109	13,202	30,482	**43,793**

Previous national-scale EGS electrical potential estimates were made for 3.5–10 km depths utilizing the Blackwell and Richards (2004a and 2004b) Geothermal Map of North America and following a similar calculation methodology (Tester et al. 2006; Augustine 2011, 2016). This detailed approach results in larger EGS energy potential for the SRP compared to previous assessments performed by Blackwell et al. (2011b). Using the same SRP boundary, the 2011 3.5 km temperature-at-depth map of the United States produces an EGS energy potential of approximately 13,800 MW_e. In contrast, this study predicts EGS energy potential of approximately 24,500 MW_e, or a 75% increase in electrical potential (Table 5). Here, the 1-km volume is centered at 3.5 km. The power potential is greater for the new map because of increased temperatures within the WSRP, which is a result of the increase in data density and removal of shallow wells. Much of the ESRP, however, has lower electricity potential because the systematic addition of the ESRPA has decreased the temperature estimates within the thickest part of the aquifer.

Table 5. Estimated Power Potential Comparison for the SRP at 3.5 km Depth

Temperature Interval (°C)	2011 Map	This Study
150–175	13,353	12,939
175–200	425	8,159
200–225		3,043
225–250		351
250–275		
275–300		
Totals	13,778	24,492

1.6 Discussion

1.6.1 Model Parameters and Potential Error

Several model parameters are poorly defined, which increases uncertainty in heat flow and temperature-at-depth estimates. The model parameters, data examination, and potential error are examined more thoroughly in the companion poster (Batir et al. 2020a). A brief explanation of the largest unknowns, handling of these unknowns, and potential error in the extrapolations are discussed next.

1.6.1.1 Heat Flow Error Sources

The highest-quality heat flow values derived from equilibrium temperature logs and accompanying thermal conductivity measurements have less than 10% measurement error. This value is based on equilibrium temperature logs collected by SMU with an accuracy of ±0.01°C (Blackwell and Spafford 1987) and thermal conductivity on the divided bar having an accuracy of approximately 5% error. Measurement error, however, does not account for the potential systemic error propagation from improperly interpreted data. Shallow temperature logs that do not fully penetrate an aquifer could appear conductive, exhibiting a linear gradient to the bottom depth. This area may in fact be purely conductive because it is a low permeable section above an aquifer; however, it could be anomalously warmed or cooled from the underlying aquifer not visible in the temperature log. Data with obvious advective heat flow signatures are removed during data evaluation, but there could still be data with less obvious advective flow and unrepresentative heat flow, especially in the medium depth data. Evaluating these linear well logs for advective heat flow is problematic and requires further research.

Error in BHT-derived heat flow values are from both the geothermal gradient and the thermal conductivity estimation. Geothermal gradients are ±20% accurate based on the compound error from the generalized surface temperature and unequilibrated BHT temperatures (Blackwell et al. 2010). The thermal conductivity values are approximately ±25% accurate based on the accuracy of the two inputs—a stratigraphic column for the well from surface to the depth of BHT and the assigned thermal conductivity for each lithology encountered. The generalized stratigraphic columns are developed from deep wells, which are few and geographically far apart, which limits the ability to interpolate thinning of basalt layers and stratigraphy changes. For example, the variation in percent of sedimentary rocks in the upper 2 km within the WSRP's generalized stratigraphic column for the Upper Deer Flat 11-19, the J.N. James 1, and the ORE-IDA 1, are 75%, 62%, and 94%, respectively (see columns in Final Report Appendix of Batir et al. 2020b). This small set of deep wells show unknown variability in the stratigraphic column that could propagate approximately ±20% error in the assigned lithology and respective thickness. The important question then becomes: how significant are the stratigraphy changes to a generalized thermal conductivity model? The significance of the stratigraphy depends on the difference in thermal conductivity for the two primary stratigraphic rocks, the sedimentary section versus the basalt.

Thermal conductivity is measured for basalt throughout the SRP, but only in a few locations for sedimentary rocks, in wells associated with the Vale geothermal anomaly and the ORE-IDA 1 well. The sedimentary rock average is 1.8 ±0.4 W/m*K, with a range from 1.1 to 2.65 W/m*K ($n = 18$). The basalt average is 1.8 ±0.3 W/m*K, with a range of 1.1 to 2.3 W/m*K ($n = 28$), but it

also shows a clear decrease in thermal conductivity with increasing depth. Although there is a low sample count for thermal conductivity measurements, these similar thermal conductivity values regardless of rock type suggest that the error should be approximately ±25%, the standard deviation of the measured values.

1.6.1.2 Temperature-at-Depth Error Sources

The largest unknown input for the entire SRP is the crustal structure of the upper 10–20 km, specifically for estimating upper crust thickness and the heat generation. Upper crustal felsic rocks produce the majority of radiogenic heat production within the Earth and are the basis for the heat flow versus heat production, the Q-A relationship, utilized in this study (see Section 2.6 for details). There is not an established Q-A relationship for the SRP; rather, the original Q-A relationship (Roy et al. 1968) is assumed accurate for estimating the radiogenic heat production component of terrestrial heat flow. As explained in the methodology, the thickness of the heat-producing layer, *b*, is assumed to be 7.5 ±2.5 km based on recent seismic interpretations (Harper 2018), and A is calculated for each individual well to satisfy the Q-A relationship. Previous estimates of the thickness of the upper crust range from 0–10 km depending on the study and location in the SRP (Hill and Pakiser 1967; Sparlin 1981). These values were used in previous SRP thermal modeling (Brott et al. 1978; Brott et al. 1981; Blackwell 1989, 1992). To understand the impact of basement depth, both b = 7.5 and 10 km are used for this study. The 4-km temperatures varied by ±7°C (hotter for b = 10 km), equivalent to a maximum of 6% error due to b thickness.

The radiogenic heat production of the upper crust, A, is another unknown. In this study, the values of A range from 0 to 15 $\mu W/m^3$, with an average of 5.3 ± 4.3 $\mu W/m^3$ in the model in order to satisfy the Q-A relationship. Calculated A values from a worldwide data set of whole rock geochemistry of igneous rocks range from 0–11 $\mu W/m^3$ (Hasterok and Webb 2017) and range from 0–4.5 $\mu W/m^3$ with an average of 3.2 ± 0.8 $\mu W/m^3$ for whole rock geochemistry samples in the SRP (Hildreth et al. 1991; Troch et al. 2017; Colón 2018). The current thermal model is overestimating heat production. Two ways to make the modeled A value match the calculated A from rock samples are: (1) increase b, which redistributes the heat production to deeper parts of the crust, or (2) include an additional heat source such as advection or higher basal heat flow. Seismic data do not support a thicker b layer, which suggests heat in the SRP could be coming from either basal heat flow or an advective heat source.

1.6.2 Comparison with Previous Work

Recent studies in the SRP include the Geothermal Play Fairway Analysis (GPFA) (DeAngelo et al. 2016), a FORGE site feasibility study (Podgorney et al. 2016), and the SMU Geothermal Laboratory Heat Flow Map of the Conterminous United States (Blackwell et al. 2011a). Both the GPFA and FORGE projects utilized the Blackwell et al. (2011a) results as the primary or one of the primary heat flow data sets to assess temperature and thermal energy potential. The GPFA went beyond heat flow by incorporating multiple heat source indicators to their heat favorability map (DeAngelo et al. 2016). The GPFA, counterintuitively, did not find a direct relationship between geothermal potential and proximity of the current Yellowstone Hotspot location. That can be explained by the variety of different indicators used in the GPFA beyond well heat flow, e.g., volcanic vents distribution, groundwater temperature, and He isotope composition and geothermometry of hot spring and well waters (Shervais et al. 2020). The 2011 SMU Geothermal

Laboratory Heat Flow Map of the Conterminous United States utilized wellbore data when available, and contour control points based on geology where heat flow measurements were not available, similar to the expert-driven weighting approach utilized for the GPFA (DeAngelo et al. 2016). The 2011 SMU temperature maps show the expected direct relationship of thermal energy potential to the proximity to the Yellowstone Hotspot, east of the northeastern terminus of the SRP. The newest heat flow map is similar to the 2011 SMU heat flow map in that they show a loose correlation between proximity to the Yellowstone Hotspot and geothermal potential. With that said, there continues to be a discussion as to how much heat is still retained in the rocks from past and any present hotspot activity. The 2020 temperature-at-depth maps show the ESRP with cooler temperatures, and the localized high temperatures could merely be from misinterpreted advective fluid flow along deep faults. These shallow high temperatures make the sites possible targets for geothermal resource projects based on reduced drilling expense.

Comparing the new 3.5-km SMU temperature map (Figure 12b) with the 2011 map (Figure 12a), the new map differs in that the model utilizes the bottom depth of the ESRPA as the upper thermal boundary condition in the ESRP, thereby producing more variability in the temperatures. A large portion of the ESRP is now modeled to be below the EGS temperature cutoff of 150°C. This new lower temperature estimate is driven by addition of the ESRPA in conjunction with several lower heat flow values. For the WSRP, the new 3.5-km temperature map is also more variable from the increased data and an updated thermal conductivity model. With the changes in the modeling, there is increased ability to compare results with complementary geophysical data. Still, geophysical studies cannot predict temperature at depths below 4 km, so drilling wells and measuring downhole temperature is the only way to truly validate the heat flow models.

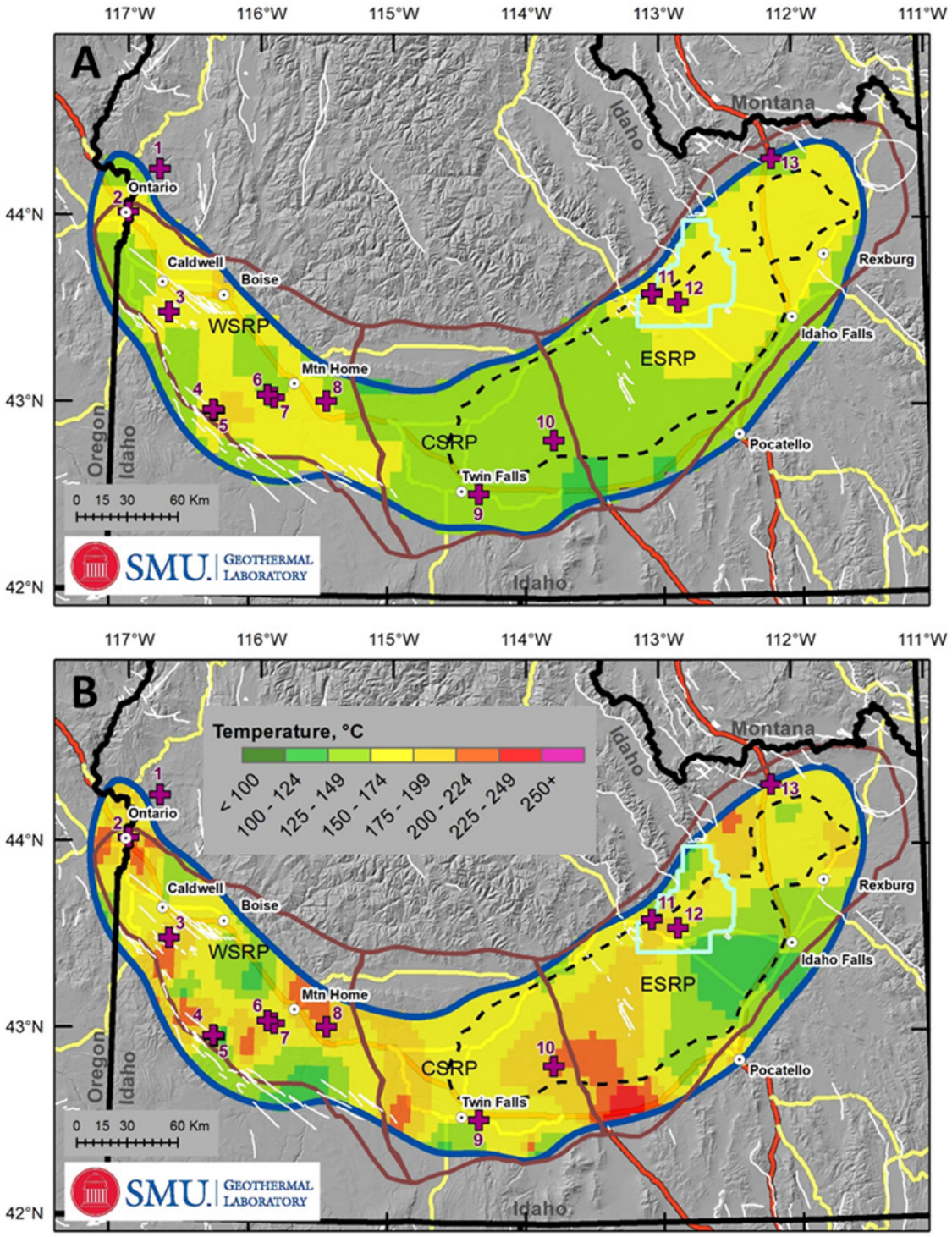

Figure 12. Comparison of temperature maps for 3.5 km depth.

(A) SMU 2011 temperature-at-depth map at 3.5 km depth (Blackwell et al. 2011b).
(B) New temperature-at-depth map at 3.5 km produced for this study.

1.6.3 Additional Thoughts

The early eruptions of the SRP are felsic, so the geologic section is characteristically younger basalt over rhyolite or sediments and rhyolite on the margins, particularly the southern margins. Felsic/rhyolitic volcanic rocks typically are low in permeability except where fractured. The opposite is true for mafic/basaltic volcanic rocks where thin lava flow sequences are highly porous along their flow surfaces, making them excellent aquifers. Yet, fluid flow in these felsic rocks is as pervasive as the young, unaltered basalts above them and along the margins. Thus, the temperatures of the felsic sections tend to also be isothermal from fluid flow, as are the basalt sections. The main difference between the felsic and basalt fluid flow within the SRP is that the felsic sections are often capped by sedimentary rocks, which decreases hydrological communication with the surface. This decreased hydrological communication and regional dip of felsic units toward the center of the SRP produces an elevated thermal regime in the center with a shallow to slightly artesian water table characterized by isothermal temperature profiles that range from 30° to 80°C for the upper 1,500 m.

This phenomenon is visible in the CSRP where felsic rocks contain isothermal sections several thousand feet thick, as demonstrated in the Kimberly well and in the deep Grandview area wells (Blackwell et al. 1992; Utah State University 2014b). In the ESRP, it is the basalts that form the aquifer, creating isothermal temperature profiles, although the temperatures in the ESRP are at or near shallow groundwater temperatures, ranging from 9° to 20°C to 1,200 m (McLing et al. 2016; Lachmar et al. 2017). This is less visible within the WSRP because of the thicker sedimentary section. These typical fluid flow characteristics of the basalt and rhyolite sections make geothermal assessment of the SRP regional area more difficult because wells deeper than 1.5 km are necessary to fully determine crustal thermal regimes. Thus, the few deep wells that do exist take on particularly important meaning for geothermal assessment despite their significant spatial separation.

For the modeling to calculate temperatures-at-depth, the heat flow versus radiogenic heat production (Q-A relationship) is an oversimplification of the total terrestrial heat flow for the SRP. The A value outputs from the thermal model for certain wells require either a higher radiogenic heat production than what whole rock geochemistry suggests (0–4.5 $\mu W/m^3$) or a thicker crust than what seismic studies for the area indicate (0–8 km). In order for the observed heat flow values to agree with whole rock geochemistry and seismic-derived upper crustal thickness, the observed heat flow requires an additional heat component such as higher mantle heat flow, advective heat transfer within the crust (faults), basin wide heat refraction, or a combination of all. As an example, the Kimama well has a 123 mW/m^2 heat flow. If mantle heat flow is 60, then 63 mW/m^2 heat must be coming from radiogenic heat production? That would require 6.3 µW/m3 of heat production and 10 km of heat-producing crust—neither of which fits the whole rock geochemistry estimates or crustal thickness estimates from seismic studies.

The work presented here focuses on direct, depth-correlated measurements to estimate heat flux and temperatures, although there are other potential temperature indicators used in the GPFA that could add insight and confidence to our estimates (Shervais et al. 2015, 2020). Collecting geothermometry of produced fluids from the high-temperature areas could be used to test the plausibility of these modeled temperatures. A spatial correlation of hot spring and groundwater temperatures to nearby wells could help find shallow or isolated isothermal aquifers. Volcanic

vents are another potential indicator of heat, although it is still unclear whether there is enough known about each vent to quantify these heat sources.

1.6.4 Suggested Next Steps

Additional data collection is necessary to further refine assumptions in this model and to resolve remaining questions. Following is a list of suggested future studies, with descriptions of how each would aid in geothermal exploration and thermal regime modeling.

1. New seismic studies that focus on mapping the location and thickness of upper crust in the SRP. This would reduce the uncertainty in the utilized *b* value and produce more understanding of the Q-A relationship of the SRP, if this is a valid and applicable relationship for this region.
2. Deep drilling in the ESRP that completely penetrates below the ESRPA, records a linear (conductive) gradient for at least 100 m, and possibly drills into the felsic rocks. Such a well would increase heat flow and basement knowledge in a region that lacks sufficient data coverage because of the expansive ESRPA. Suggested well locations are along the south and/or east margin of the ESRPA, such as between Pocatello and Idaho Falls or northwest of Rexburg.
3. Deep wells both northwest and northeast of Rexburg would also increase understanding of lithospheric cooling along the Yellowstone Hotspot track that would aid in large-scale, time-dependent, volcanism age-driven thermal regime models.
4. To the north of the SRP, outside this project focus, is the Central Idaho Basin and Range. This area was cited by Blackwell (1989) as a potential geothermal resource zone, yet no additional data collection or analysis were ever completed. With the focus on EGS and new interest in sedimentary basins for geothermal EGS, this region continues to be a possible area for exploration.

1.7 Conclusions

This study produced increased resolution of the thermal regime of the WSRP and a better understanding of the thermal regime controls in the greater SRP region. Although limited new well data are available for the CSRP and ESRP regions, the additional well data coverage for WSRP allows for at least one data point within any ~15 km gridding radius circle. Comparing the geothermal resource evaluation work from the 1970s and 1980s, it is surprising to see many areas with high-temperature wells still not included in assessments by government or private exploration. The areas along the edges of the SRP are complicated, with fault-related fluid flow and complex crustal structure, yet are prospective for both conventional geothermal (power and direct use) and EGS development. The elephant in the room, the ESRPA, is modeled with a high heat source below, but until additional wells penetrate to depths below 1 km, the proportion of that heat being advectively carried away by the aquifer will remain unknown, along with the full geothermal resource potential. The thermal potential results from this study show electricity potential (≥150°C) within the 1 km to 4 km depths as approximately 44,000 MW_e. At 3.5 km depth, power potential is 75% greater based on the new temperature-at-depth maps compared to the same area within SMU's 2011 U.S. temperature map, even with the removal of the area within the ESRPA.

2 Uncertainty Analysis of Subsurface Temperature Estimates in the Snake River Plain

2.1 Abstract

Estimating subsurface temperature always entails some degree of uncertainty. This paper assesses uncertainty associated with recent SRP subsurface temperature estimations based on heat flow and a radiogenic heat production model. Heat flow data vary in abundance, spatial and depth distribution, and quality. We examined data attributes (including quality, location, and fault proximity) and quantified heat flow interpolation variability. Results show initial data processing and selection of regionally representative data are most important to reduce interpolation uncertainty. Data removal using a 2.5-km fault trace buffer is appropriate to inhibit potential advective heat flux, whereas a 5-km buffer is too much, such that it produces random changes in the heat flow grid. Fault buffers change mapped heat flow by less than 20% in most areas of the SRP. Additional temperature-at-depth calculation uncertainty is from the radiogenic heat production model, which follows the heat flow-radiogenic heat production (Q-A) relationship. Model sensitivity to the radiogenic heat production model is tested by varying heat production layer thickness from 5 km to 10 km and examining temperature change at 4 km. Temperatures vary by 10% (up to 27°C), although most temperature change is less than 5%. Examination of heat flow, upper crustal thickness, and whole rock geochemistry revealed the Q-A relationship may be an oversimplification of the SRP thermal regime. Radiogenic heat production is approximately 12 to 40 mW/m² for this region, and mantle heat flux is set at 60 mW/m². Therefore, measured heat flow above 100 mW/m² is unaccounted for in the Q-A relationship and must derive from an additional heat source. This anomalous heat flux may be heat refraction, advection, additional mantle heat flux, or a combination. Many data sites along the SRP margins and in the ESRP contain anomalous heat flow, whereas the WSRP is generally lower than the 100 mW/m² cutoff.

2.2 Introduction

Wells are drilled for a variety of purposes (e.g., oil and gas exploration, water wells, geothermal exploration) in a variety of geologic environments. Upon drilling completion, the type of well data (temperature, depth, and lithology) also varies depending on industry timeframe and equipment type. So, “temperature logging” of a well can mean anything from one BHT while drilling, to the opposite extreme of many temperatures along the well length after well completion (possibly at equilibrium). These differences in data collection make it difficult to work with the basic parameters of temperature and depth in an analysis. Even the assignment of data quality can vary between researchers. Many of the wells within the SMU Geothermal Laboratory Heat Flow database are assigned quality values. The majority of other data do not have an assigned quality, and that is the norm for most related data. Therefore, this paper discusses the process of reviewing data, assigning quality, and the significance of the different parameters on the final product, maps, and geothermal resource potential calculations.

This study is based on research completed as part of an SRP project to examine the regional heat flow and resulting estimations of geothermal resource potential. A separate paper (Batir et al. 2020c) discusses in detail the data collection, geologic setting, methods, and resulting resources,

whereas this paper goes into detail about the impact of the upfront data collection, filtering, gridding methods, and geological parameter decisions on the final maps.

2.3 Data Collection and Filtering

The data collection included 926 wells with at least temperature and depth data, and additionally heat flow and lithology data from the National Geothermal Data System, the Idaho Oil and Gas Conservation Commission's database, and the SMU Geothermal Lab Heat Flow database. For well sites with more than one temperature or heat flow value, the most representative, highest-quality value was used to represent the site regional-thermal regime. For wells with only temperature and depth data, a heat flow value was calculated based on the local lithology (to assign a thermal conductivity) and surface temperature (to assign a well gradient). The heat flow value at each site is considered the primary parameter for inclusion in the calculations (Batir et al. 2020c).

Data in the SMU Heat Flow database are assigned a quality code: A, B, C, D, X, or G (Table 6). The classification is based on a heat flow standard developed in the 1970s (Blackwell et al. 1991) and updated in 2012 to include wells from oil and gas drilling databases (Richards et al. 2012). The standard quality codes are based on the total depth of the well, length of consistent positive gradient, measured thermal conductivity from core or cuttings, temperature corrected for impact from drilling fluids, terrain, etc., and whether it is located in a known geothermal resource area or regional setting. With the inclusion of the oil and gas data, these quality codes were updated to incorporate the proximity to other well sites for related errors (thus a cluster of wells is expected to be within one standard deviation of each other) with codes: BHT-C, BHT-D, or BHT-X.

Table 6. SMU Heat Flow Database Quality Criteria (modified from Blackwell et al. 1991)

Quality Code	Description (From Richards et al. 2012)	Estimated Error
A	High Quality: >100 m depth with >50 m linear gradient	<10%
B	Medium Quality: >50 m depth, some problems	10%–20%
C	Poor Quality: Shallow, isothermal	>20%
D	Check Again: not used in resource assessments	--
X	No Hope: not used in resource assessments	--
G	Geothermal System: not used in regional mapping	--
BHT-C	BHT Derived: within 1 standard deviation of nearby data	~25%
BHT-D	BHT Derived: greater than 1 standard deviation of nearby data	>25%
BHT-X	Isolated point and anomalously high or low	--

The study determined the temperatures between 1 km and 4 km and the related thermal regime within that zone. The SRP is unique in that the shallow data are highly impacted by the high-flow aquifers. Therefore, without consideration of any of the quality codes previously assigned, data shallower than 125 m were removed upfront to eliminate the localized shallow thermal

regime and allow us to focus on the deeper regimes. The data then went through a series of reviews to “make the cut” to be in the final heat flow data set.

The heat flow data were filtered to include only sites representative of the study area’s conductive thermal regime. This meant removal of heat flow sites beyond the range of 45 to 175 mW/m². Data below 45 mW/m² are too low for the expected mantle heat flow (45–60 mW/m²) (Blackwell et al. 1991; also, Section 1.4.1.3 of this study). Heat flow sites above 175 mW/m² are considered part of a localized hydrothermal geothermal system and therefore not representative of the regional SRP thermal regime.

Well sites with a heat flow quality of D and X were removed. The sites considered marginal (C and G) were not used if another higher-quality well is nearby (within gridding area 5’x5’). Wells of C and G quality that passed the additional temperature data criteria for this project were kept as they are representative of the conductive SRP thermal regime (see Section 1, Table 1). After mapping the heat flow values, isolated data points outside one standard deviation of the SRP average heat flow of 90 ±20 mW/m² were examined again and removed.

BHT sites had their own set of quality limitations. The minimum depth for oil and gas well BHTs was 600 m. Each well temperature was plotted with the surrounding BHT cluster of wells within a 15-km radius; if the temperature was within 1 standard deviation of the cluster then BHT-C was assigned, and if >1 standard deviation then BHT-D was assigned. Wells isolated (no other well within a 15-km radius) were assigned a BHT-X quality code. Only the BHT-C sites were used in the final data set.

From the initial 926 well sites, 206 final heat flow sites were used to determine the temperature-at-depth extrapolations from 1 km to 4 km depths (Figure 13). Approximately half of these sites are A or B quality, and half are BHT-C, with a smaller number of C and G quality sites (Table 7). In the end, all the different ways to filter the data reduced the number of data sites by 75%. In doing so, the data set is considered a high-quality one that may represent a conservative estimate of heat flow and temperature-at-depth, yet is also expected to be more accurate in areas with data.

Table 7. Heat Flow Sites by Data Quality

Data Quality	Number of Sites
A	40
B	54
C	16
G	4
BHT-C	92

As part of the gridding process, there were two tiers of well sites based on proximity to the UGSG SRP boundary line. The first group of 161 wells are in the SRP and within a 20-km surrounding boundary buffer zone (Figure 13, yellow circles). The second group of 45 sites fill

the map edges for gridding, in addition to providing lithology information (Figure 13, light blue circles).

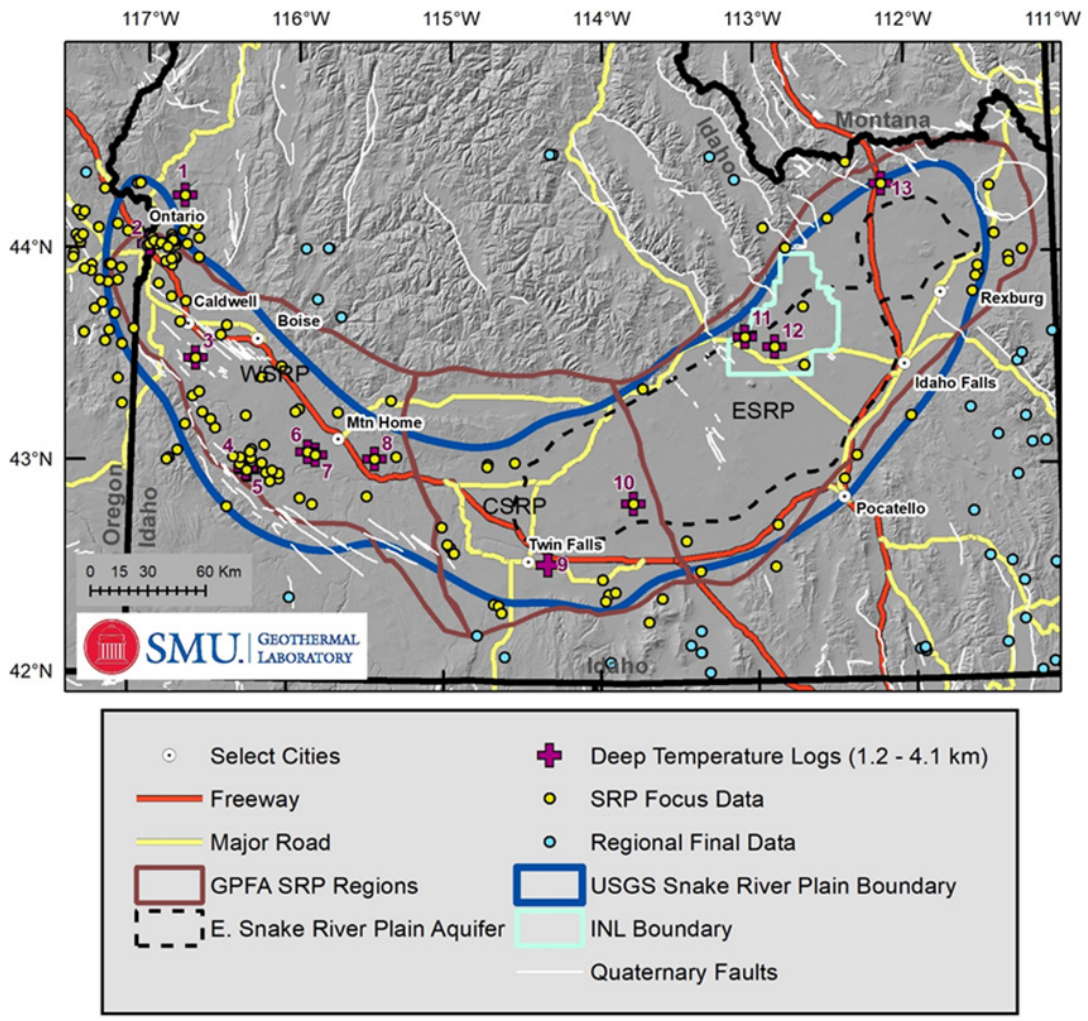

Figure 13. Final data locations utilized for heat flow mapping and temperature-at-depth extrapolations. Yellow data points are within or <20 km beyond the USGS SRP boundary line. Light blue points are heat flow sites near the study area for regional heat flow correlation.

2.4 Interpolation Algorithms and Disparate Data

The heat flow and temperature-at-depth maps are produced by interpolating individual heat flow measurements into a contoured surface. For this study, ESRI ArcMap 10.6 was used for the heat flow interpolation, using the Spatial Analyst Toolbox (Environmental Systems Research Institute 2019). Grid cells are 5 km x 5 km, and the data search radius is 15 km. Determination of the most appropriate interpolation tool was not a straightforward task, considering the goal of incorporating the spatial and geologic dependence of heat flow data with representative maps of the geology in the study area. Stutz et al. (2015) and Aguirre et al. (2013) presented improved heat flow and temperature mapping, utilizing the kriging tool that incorporated a regionally specific semivariogram for defining the constraints on interpolation within the Appalachian

Basin. A kriging semivariogram did not show a spatial correlation within the SRP data because of low and disparate data density. Therefore, we examined kriging (where data exist), spline, inverse distance weighting, and natural neighbor to determine the most accurate and complete spatial display of the data. A side-by-side comparison highlights key differences in these four interpolation methods (Figure 14). The inverse distance weighting and kriging methods allow for spatially limited grids, only gridding where cells are data supported. These two methods minimize overinterpretation, but produce single-point, potentially erroneous, anomalies from isolated data. Conversely, the spline and natural neighbor methods produce a complete raster within the entire mapped extent by varying the search radius for each grid cell. Visible, potentially erroneous, variations between the spline and natural neighbor method occur in the ESRP and CSRP where there are only a few data points. The spline interpolation minimizes contour curvature, whereas natural neighbor does not; thus, it may introduce complexity in the gridded values.

The percent difference between these four tested interpolations include: kriging versus inverse distance weighting, spline versus natural neighbor, and kriging versus spline (Figure 15). Nearly all cell values are within 20% difference between the kriging and inverse distance weighting interpolation, approximately equivalent to the error of the B-quality heat flow sites. The largest differences are along the margins in the ESRP where there are high heat flow values juxtaposed with lower heat flow. Because the data spatial dependence (via the semivariogram) could not be determined, the kriging interpolation produces a simple average, whereas the inverse distance weighting, by using distance from cell center, may introduce irrelevant distance weighting. The spline versus natural neighbor interpolations show large percent differences in gridding zones between two far apart data points. Again, most of the gridding shows variability less than 20%, but certain areas have up to 40% difference, mainly when gridding non-data areas between data points with a large heat flow value difference.

It is difficult to say which method is most appropriate because of the lack of data. Here, the spline interpolation method is chosen because the minimum curvature represents the data that are known, rather than adding unrealistic complexity to the final grids. Kriging, compared to spline interpolation, also shows that the majority of difference is within 20% in high-data-density areas, although there is a higher maximum difference of 70% versus the previous 40%. The higher percent difference highlights the issue of data density. Where there is only one data point, kriging interpolation produces a single value circle the size of the 15-km search radius, whereas spline interpolation incorporates other data into gridding, connecting isolated values to nearby values and producing a complete and continuous grid, which also produces zones that are purely interpolation. Resource estimation was performed using spline interpolation because of the need for a complete and continuous grid; however, we use kriging interpolation to assess uncertainty in heat flow mapping and temperature-at-depth calculations associated with the input heat flow data.

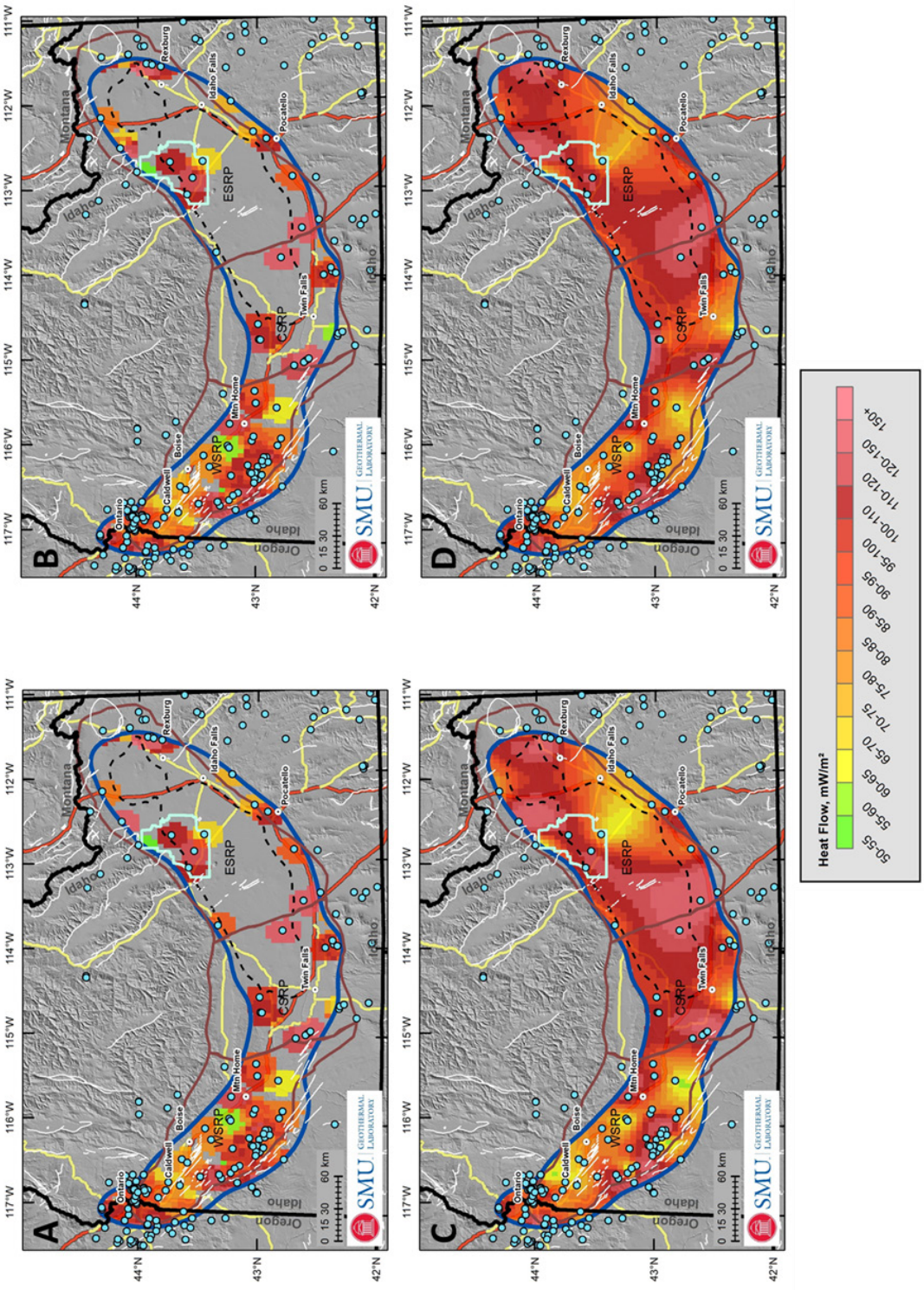

Figure 14. Comparison of interpolation methods for gridding: (A) kriging, (B) inverse distance weighting, (C) spline, and (D) natural neighbor. The kriging and inverse distance weighting allow for limiting interpolation to a given search radius (here, 15 km) as opposed to spline and natural neighbor, which interpolate all grid cells, including those without data support.

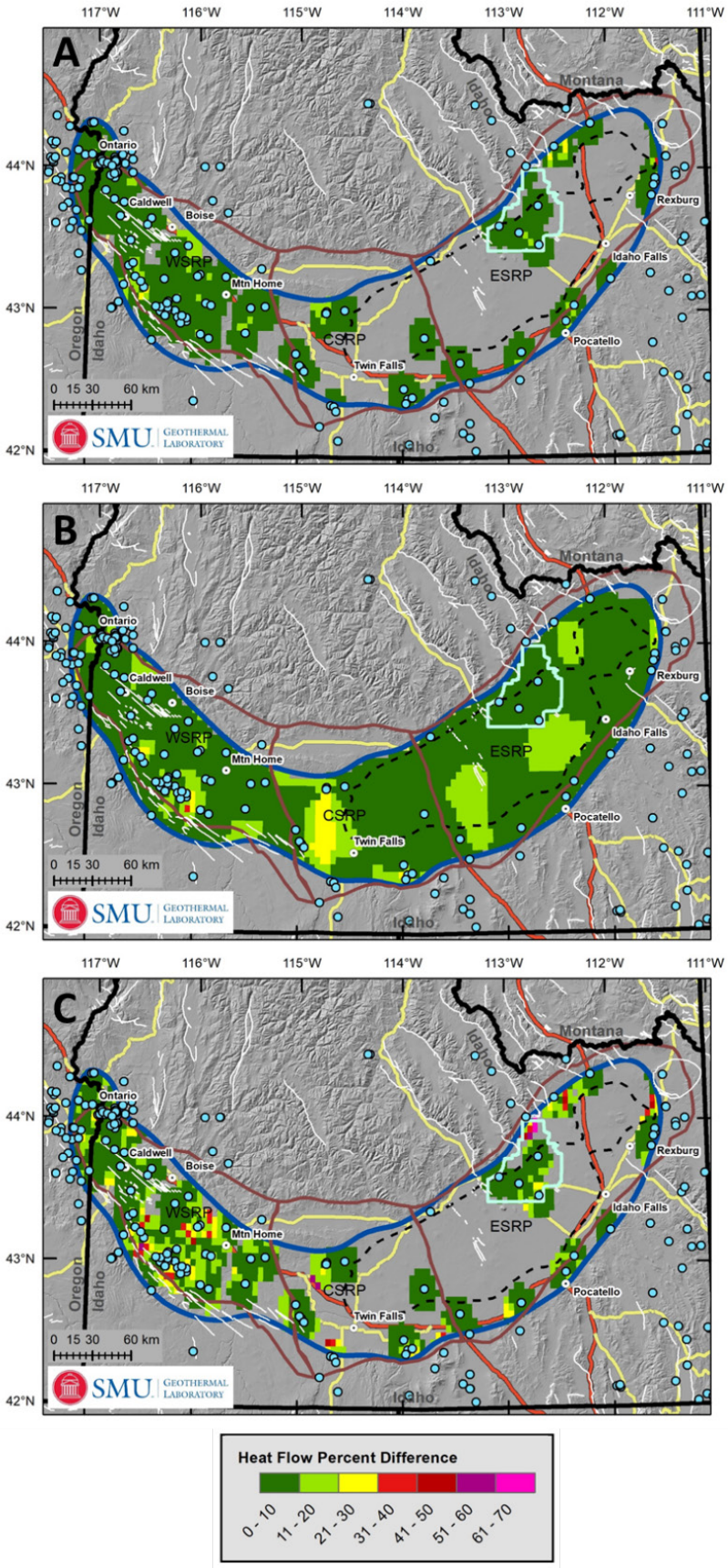

Figure 15. Comparison of differences between gridding methods.

(A) Kriging interpolation minus inverse distance weighting interpolation percent difference. Nearly all grid cells are within 20% of each other, within the error of most heat flow values.

(B) Natural neighbor interpolation minus spline interpolation percent difference. Areas with the most difference are zones with no data. The areas with the highest differences include the northeastern ESRP, a large section of the CSRP, and the southwestern boundary in the WSRP.

(C) Kriging interpolation minus spline interpolation percent difference. Some grid cells have up to 70% difference. These high-difference grid cells are locations where only one data point is used for kriging.

2.5 Geologic and Structural Controls on Heat Flow

The SRP contains structurally and lithologically controlled fluid flow that contributes advective heat flux to some of the measured heat flow values, which could be misrepresented as the regional thermal regime if not properly identified. Potential anomalous heat flow associated with elevation-driven fluid flow along the SRP margins and fluid flow along Quaternary faults are assessed and resulting heat flow maps compared. The ESRPA is a significant cold-water aquifer system that masks the subsurface thermal regime. Although there are temperature differences visible within the ESRPA, maximum temperatures reach only 20°C at depths of 500 m to 1,000 m (McLing et al. 2016). The heat flow values in the vicinity of the ESRPA are representative of the thermal regime below the aquifer. The pervasive flow in the aquifer masks the thermal regime, and any geothermal energy production will require drilling through the aquifer system (McLing et al. 2016).

2.5.1 Heat Refraction Along Margins

Blackwell (1989) and others observed higher heat flow on the margins of the WSRP compared to the central axis of the WSRP (Brott et al. 1978). This phenomenon was attributed to heat refraction deflecting heat from the low-thermal-conductivity basalt and sediments to the high-thermal-conductivity granites and rhyolites that make up the rocks of the Owyhee Plateau and Idaho Batholith on the margins of the WSRP. This heat flow pattern is still visible in the mapping of heat flow, shown by a cross section across the WSRP, where high heat flow is observed along the margins compared to the central axis of the basin structure (Figure 16). Although this observation is still valid, additional BHT-derived heat flow reduces the signature of this phenomena. There are approximately 20 new heat flow measurements in the central portion of the far WSRP near the Oregon-Idaho border and 18 new heat flow measurements along the Owyhee Plateau-SRP margin. The new heat flow values average is 103 ±14 mW/m², and 91 ±20 mW/m², respectively. These averages are within one standard deviation of the Blackwell (1989) WSRP average of 99 ± 4 mW/m², yet show that variability occurs depending on location of measurements within the SRP.

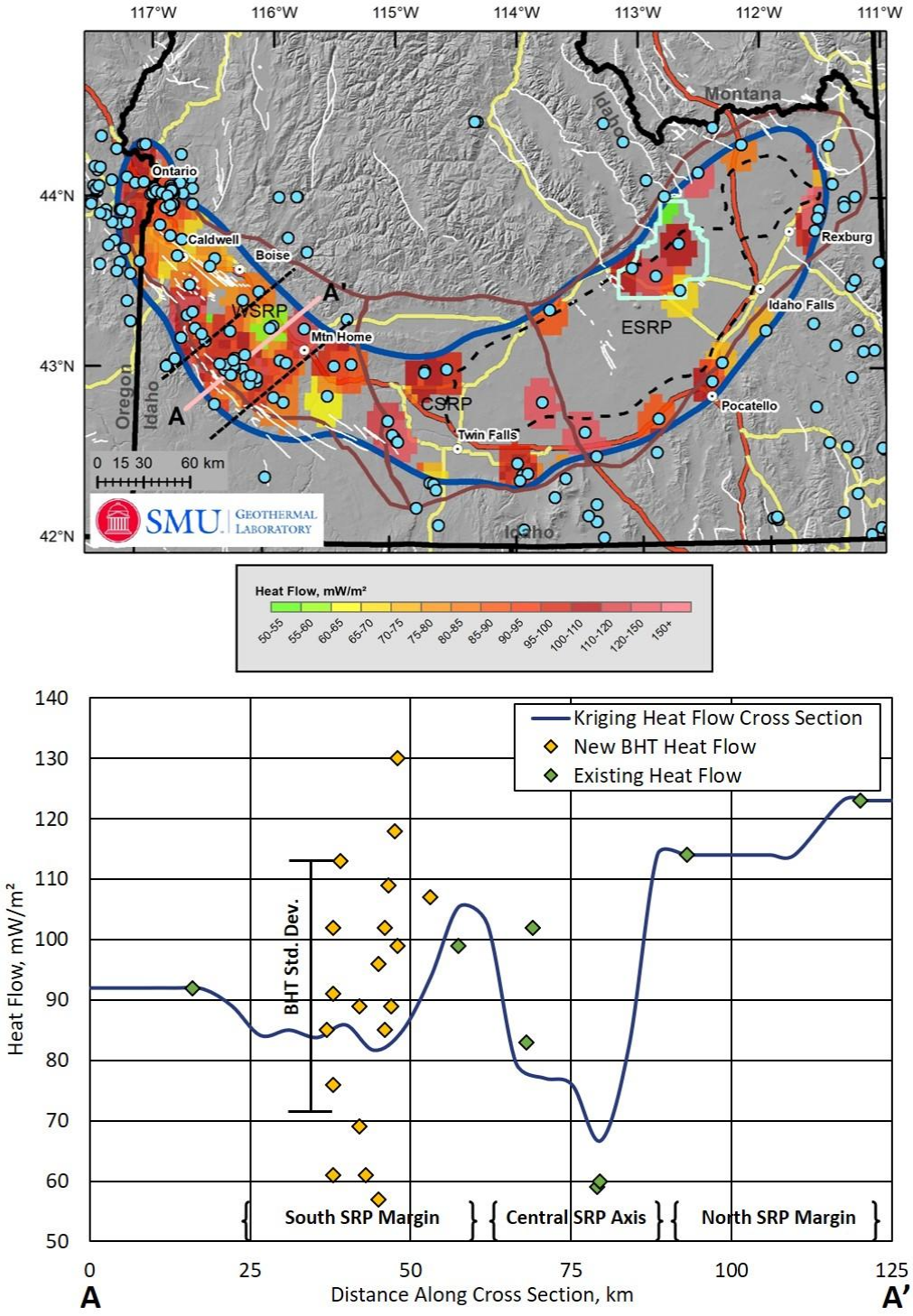

Figure 16. Kriging heat flow map with A-A' heat flow cross section location. Data within 25 km of the cross section line, indicated by the black dashed lines, are plotted on the graph.

In general, heat flow is higher on the margins of the SRP compared to along the central axis, although many of the values are within one standard deviation of each other. New BHT data along the southern margin are highly variable, with an average heat flow of 91 ±20 mW/m². The high variability is likely due to drilling disturbances, but may also have a geologic explanation such as unmapped faults.

2.5.2 Heat Flow Variation Along Quaternary Faults

Quaternary faults were used in several GPFA projects as an indicator of permeability (Faulds et al. 2013; Shervais et al. 2015). If true, increased permeability and resulting fluid flow along faults would result in a lower or higher observed heat flow value not representative of the regional conductive thermal regime, but instead representative of a present day transient local thermal regime. Determination of the advective heat flow component within the SRP is complicated because the 206 heat-flow-site database entries used here include either (1) temperature logs that exhibit a linear geothermal gradient—suggestive of a conductive thermal regime—and do not record obvious fluid flow indicators such as an isothermal section or temperature overturn or (2) the heat flow is derived from a BHT. Additionally, there are wells throughout the study area that are removed because of fluid flow signatures, but these wells containing an advective signature do not show an apparent correlation besides areas within the ESRPA. As an alternative method, Quaternary fault heat flow impact is assessed by removing data near faults and examining the change in observed heat flow. Data are removed at buffer intervals of 1 km, 2.5 km, and 5 km near a Quaternary fault trace. From these results, the changes in heat flow pattern are observed in Figure 17, and then the amount of change is quantified and shown in Figure 18 as a percent difference between the complete data set and the data set with data located near faults removed.

There are only 9 data points within 1 km of a Quaternary fault trace, 19 within 2.5 km, and 41 data points within 5 km of a Quaternary fault trace (Figure 17). There is little difference between the full data set and the removal of sites 1 km from faults (Figure 18a). The biggest change to the heat flow pattern is south of Caldwell, Idaho. There is one data point that is almost 15 km away from all other data that is subsequently removed in the 1-km distance filtering. With removal of this data point, the entire 15-km search radius is changed. There are several other grid cells that change greater than ±10% from the full data set value. There is a greater change in heat flow visible after removing the data around the 2.5-km fault trace. Most areas with a change in heat flow are still within ±20%, but now there is a clear pattern of alternating positive and negative heat flow change in the WSRP. The removal of data from the 5-km fault trace creates a percent difference map that does not contain an interpretable pattern, but instead heat flow seems to change more randomly. These results suggest data points within approximately 1 km to 2.5 km of a Quaternary fault trace may be most representative of highlighting an advective heat flow signature. At 5 km there is both a positive and negative change in heat flow, which suggests that there is no correlation between fault location and enhanced geothermal energy potential.

2.5.2.1 Western Snake River Plain Fault Impact

After studying the impact of removal of nearby sites to a fault, we can see that for the WSRP, the heat flow differences are both lower (green colors) and higher (yellow colors) values along the southern margin of the WSRP (Figure 18). It is worth noting that there is only a minor change along the southern margin within the 1-km zone. The minor change, however, helps to clearly show the heat flow difference of lower heat flow to the northwest along the fault zone and higher heat flow to the southeast along the fault zone. There are other small changes outside the southern margin of the WSRP, although these other visible changes show relatively minor differences when compared to the full heat flow data set.

2.5.2.2 Eastern Snake River Plain Fault Impact

There are only two data points removed in the ESRP, one site on the northern margin within the 1-km fault trace zone, and one on the southern margin between Twin Falls and Pocatello using the 5-km fault trace zone. The two data points removed are on the margin of the SRP and are isolated, further than 15 km to the nearest data point. It is important to note that the 5-km fault trace buffered data set does not have sufficient data to calculate a semivariogram using the 5-km x 5-km grid cell size and instead utilizes a 7-km x 7-km grid cell size with a 21-km search radius for overall comparison. Although there are differences visible in Figure 17 and Figure 18 because of the larger search radius, these data are outside the interpreted 15-km sphere of data influence. Therefore, removal of the two data points in the ESRP should produce less of the area to be gridded. Although there is a difference in grid values, the difference in interpolation is limited.

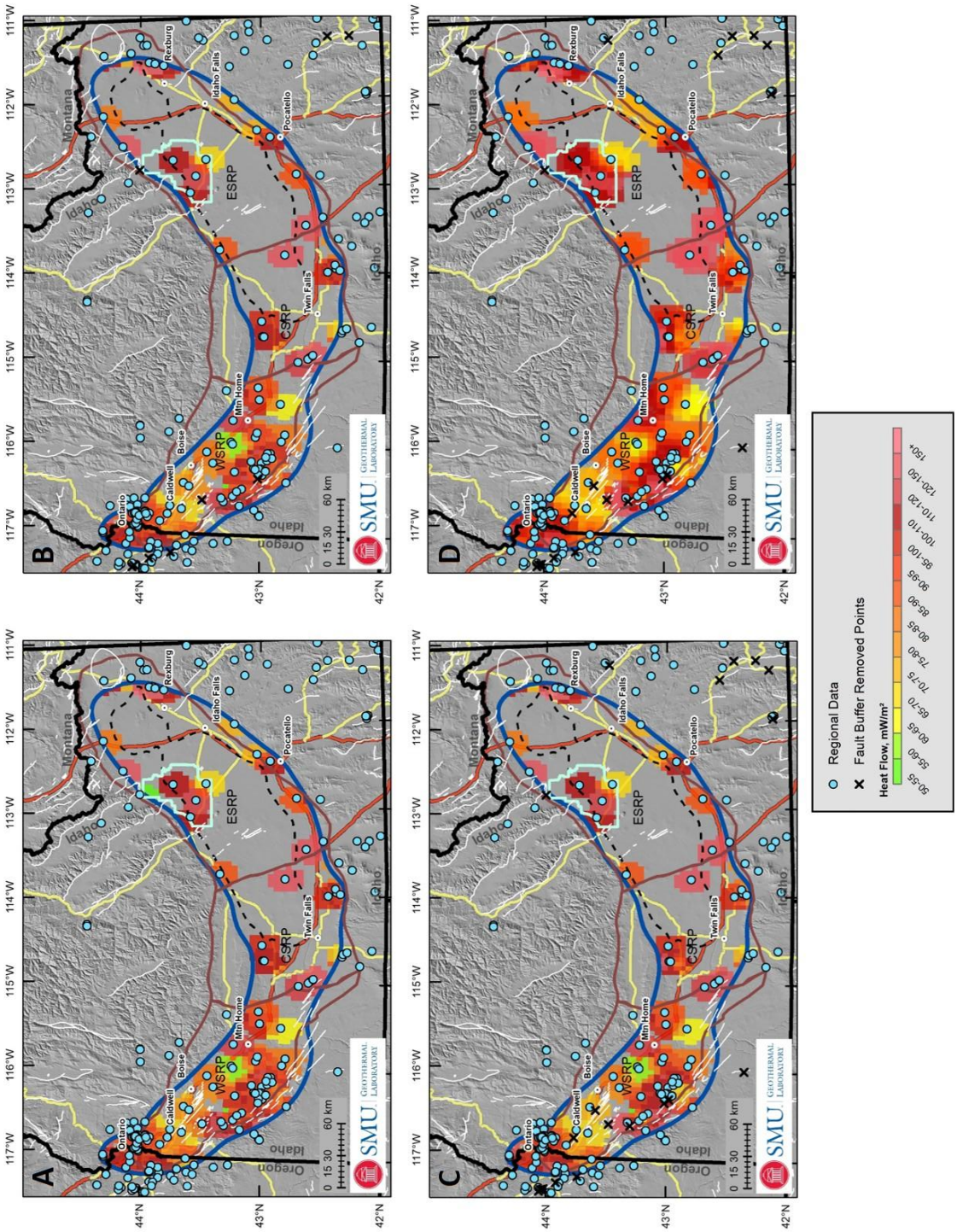

Figure 17. Visual comparison of heat flow after removal of data near faults. (A) Terrestrial heat flow map produced from regional data set. Removed data points are displayed as a black X. (B) Terrestrial heat flow after removal of wells within 1 km of Quaternary fault traces from the regional heat flow data set. (C) Terrestrial heat flow after removal of wells within 2.5 km of Quaternary fault traces from the regional heat flow data set. (D) Terrestrial heat flow after removal of wells within 5 km of Quaternary fault traces from the regional heat flow data set.

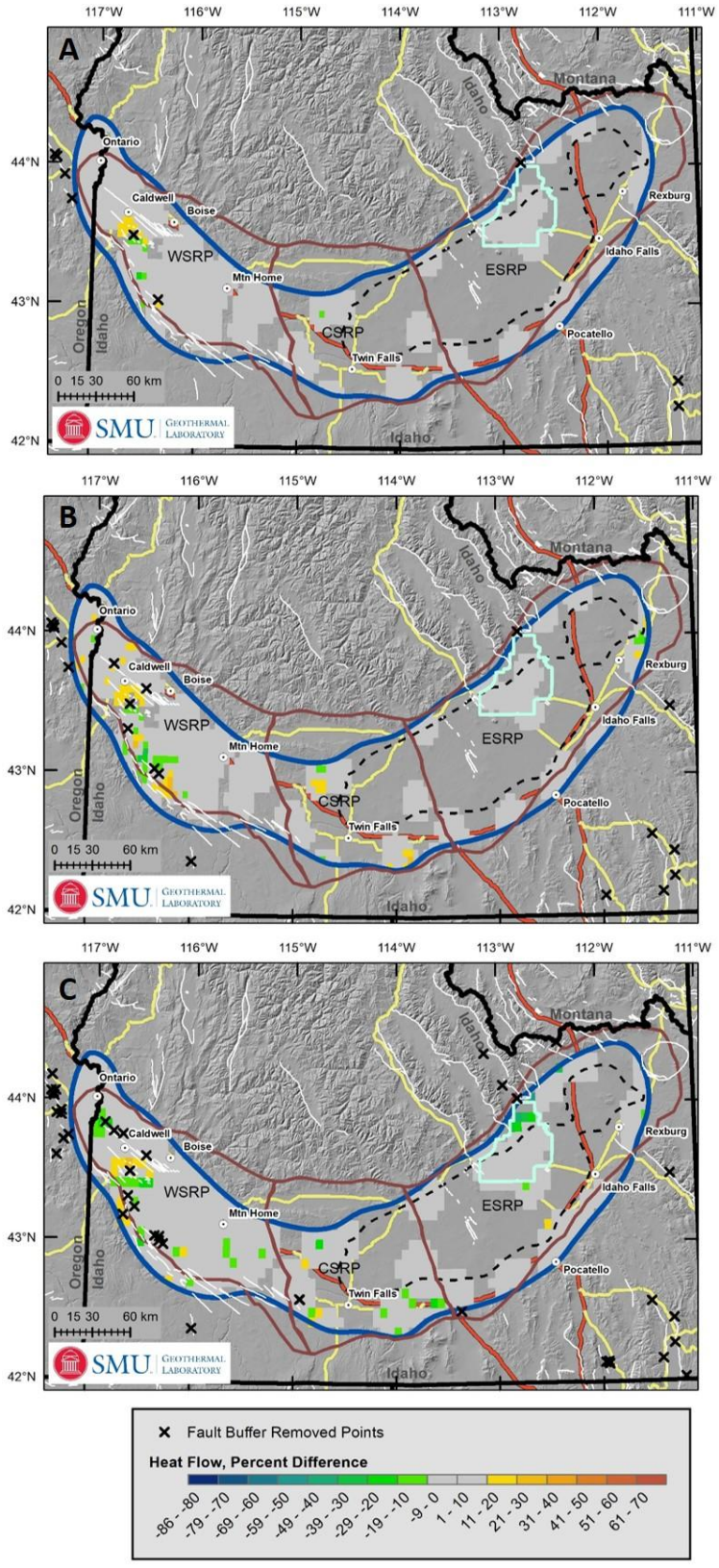

Figure 18. Heat flow percent difference comparison of near-fault data site removal.

(A) Heat flow percent difference between the regional data set and the 1-km fault trace buffer data.

(B) Heat flow percent difference between the regional data set and the 2.5-km fault trace buffer data.

(C) Heat flow percent difference between the regional data set and the 5-km fault trace buffer data.

Note that the 5-km fault trace buffered grid has a cell size of 7-km x 7-km and search radius of 21 km because the data set was too small to produce an accurate semivariogram using the 5-km by 5-km grid cells. An equivalent grid was made from the whole regional data set for this comparison. Black X's show locations of fault buffer removed data. Areas with negative heat flow difference are areas that contained high heat flow values near faults (potentially upflow, or outflow zones) and areas that are positive contained lower heat flow values (potentially downflow, or recharge zones).

2.6 Radiogenic Heat Production Layer Thickness Impact on Temperature at 4 km Depth

One of the largest unknowns for the SRP is the thickness and variability of the radiogenic heat production layer. Roy et al. (1968) and Lachenbruch (1968) described an empirical relationship between co-located measurements of the radiogenic heat production of plutonic upper crust rocks (A) and the surface heat flow (Q), which they referred to as the Q-A relationship (equation 1):

$$Q = Q_m + A(b) \quad (1)$$

where Q, Q_m, A, and *b* are the parameters for surface heat flow, mantle heat flow, radiogenic heat production, and radiogenic heat-producing layer thickness, respectively. Q and A are measured, and with sufficient data, a Q-A plot for a region can be made to determine Q_m and *b* (Blackwell 1971; Blackwell et al. 1991). Blackwell et al. (1991) calculated a *b* value of 10 km for the eastern United States, which was later modified to equation 2 to account for thick sediment cover:

If $Z_{sed} < 3$ km, then

$b = 10$ km, *else*

$$b = 13 \text{ km} - Z_{sed} \quad (2)$$

where Z_{sed} and *b* are sediment thickness and radiogenic heat production layer, respectively. This relationship is built on the assumption that the region is in steady-state and contains a *conventional* continental crust, where *b* is approximately equivalent to the upper crust thickness.

In the SRP, these assumptions (conventional crust composition and steady-state heat flow) may not be accurate because of the recent geologic history (Brott et al. 1978, 1981; Wood and Clemens 2002). Still, the SMU-Cornell temperature-at-depth calculation model accurately estimates the deepest measured temperatures (3,100 m) and predicts geologically reasonable temperatures in the upper 4 km. Note that there are 61 measured temperatures deeper than 750 m and 13 presumed equilibrium temperature logs ranging in depth from 1,200 m to 3,100 m scattered across the SRP (see Appendix B for temperature logs). Still, the impact of *b* is assessed to understand temperature uncertainty based on this unknown parameter. The *b* value is set to 5 km, 7.5 km, and 10 km (based on results from Harper [2018] and estimates used by Brott et al. [1978, 1981]), and the temperature variability at 4 km is assessed (Figure 19). The values of A and *b* set the amount and distribution of radiogenic heat production in the subsurface and will alter how temperature changes with depth. The A value is not assessed in this step because it varies proportionally with *b* to make the Q-A relationship true.

Temperature changes a maximum of 27°C (Figure 20) when testing model sensitivity to the *b* value. The temperature fluctuations of 0°–27°C represents approximately 10% uncertainty in temperature at 4 km, although most of the temperature variability is less than 5%. Based on these results, the *b* value has minimal impact on temperature-at-depth calculations, provided that *b* is within or near the range of 5 km to 10 km thick. The area with the greatest temperature change is within the INL property boundary and near Rexburg. The higher temperature difference in this region compared to others warrants further investigation.

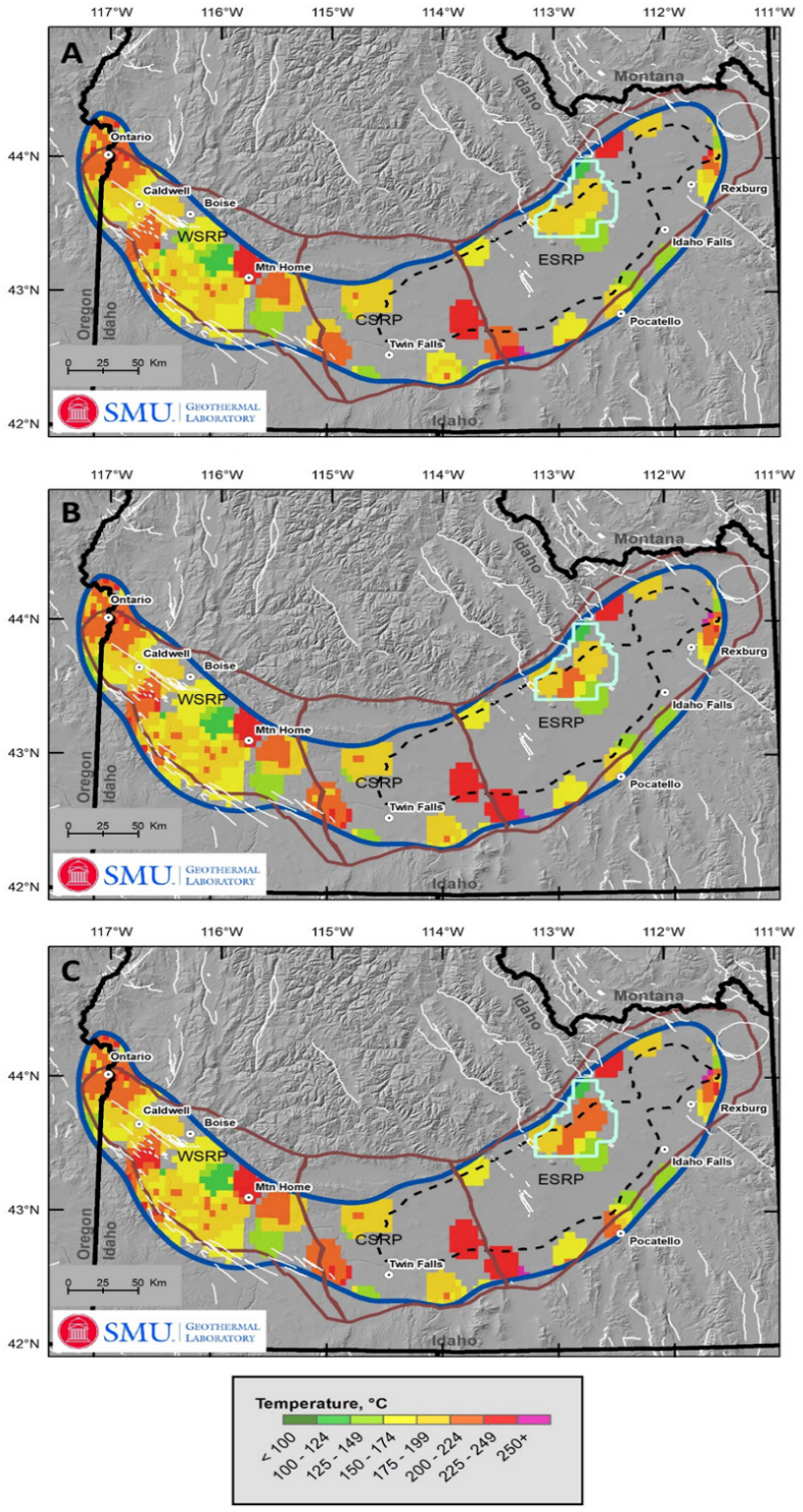

Figure 19. Temperature variations from changes in radiogenic heat production layer thickness (*b).*

(A) Temperature at 4 km depth with a radiogenic heat production layer thickness of 5 km.

(B) Temperature at 4 km depth with a radiogenic heat production layer of 7.5 km.

(C) Temperature at 4 km depth with a radiogenic heat production layer of 10 km. Temperature estimates between thickness depths change less than the color intervals shown on these maps, except for the area within the INL site and near Rexburg.

The next figure (20) shows maps of actual differences.

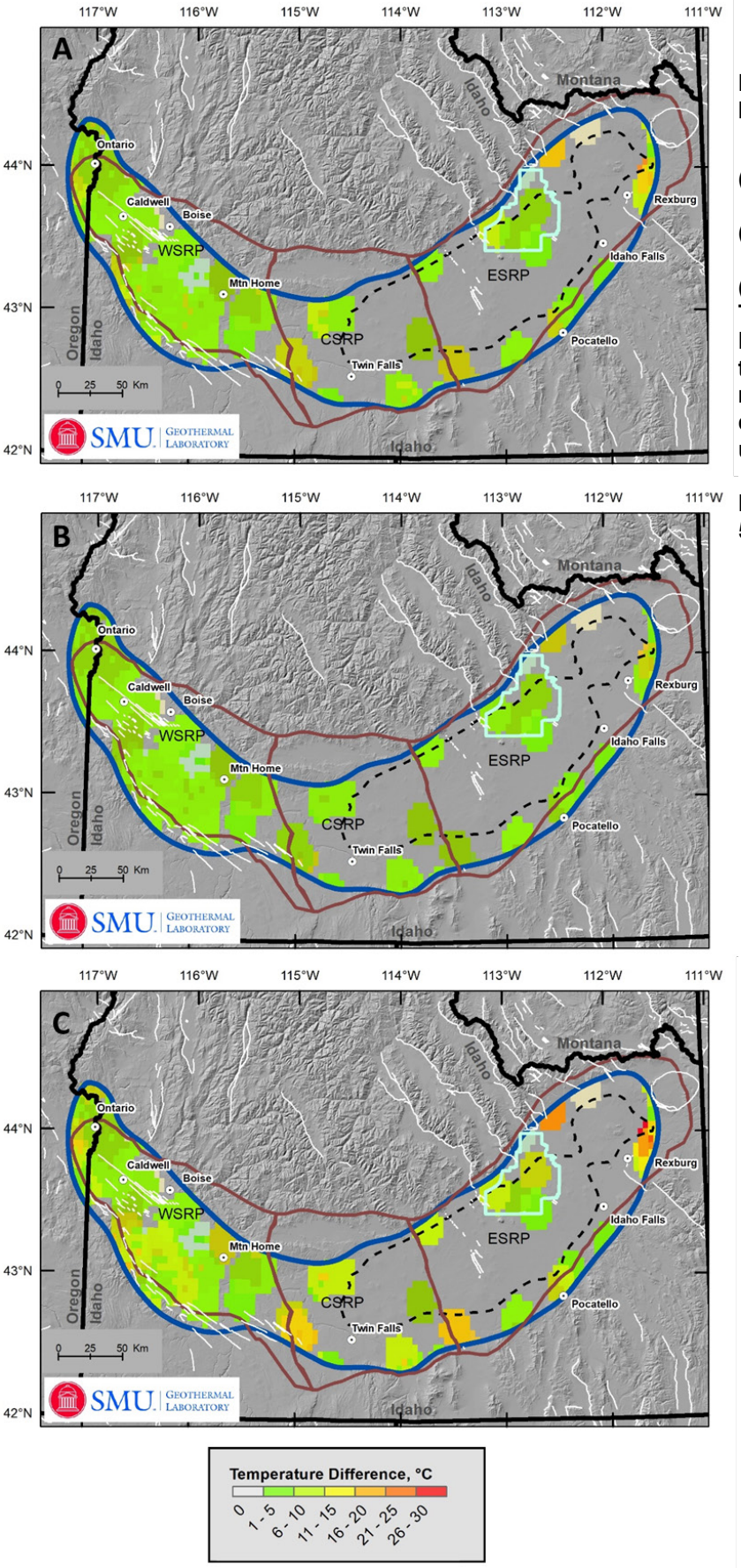

Figure 20. Differences between 4 km temperature maps (Figure 19).

(A) 7.5 km minus 5 km thickness.

(B) 10 km minus 7.5 km thickness.

(C) 10 km minus 5 km thickness. The maximum difference is near Rexburg in the 10 km minus 5 km thickness differences (28°C), while most areas have up to 15°C difference, equal to less than 5% uncertainty.

Note the average raster cell value is 5 ±4°C.

2.7 Quantifying Anomalous Heat Flow

The SRP heat flow signature is anomalously high compared to other regions and contains a heat component not accounted for by the Q-A relationship based on the measured terrestrial heat flow, the estimates of upper crust thickness, and estimated radiogenic heat production from felsic rocks within the SRP. The 1D steady-state temperature-at-depth estimates produced in this model assume the study region is dominated by conductive heat flow and the only additional heat input is from radiogenic heat production and follows the Q-A relationship (Figure 21). Data filtering explicitly removes sites with fluid flow signatures to satisfy these assumptions; however, the final regional data set still has higher heat flow and higher calculated radiogenic heat production than what whole rock geochemistry suggests is appropriate.

Whole rock geochemistry estimated A ranges of 0–4.5 $\mu W/m^3$, with an average of 3.2 ±0.8 $\mu W/m^3$ in the SRP (Hildreth et al. 1991; Troch et al. 2017; Colón 2018). Using our methodology (Stutz et al. 2015), temperature-model-calculated A ranges from 0 to 15 $\mu W/m^3$, with an average 5.3 ±4.3 $\mu W/m^3$. Worldwide heat production measurements range from 0–11 $\mu W/m^3$ (Hasterok and Webb 2017), meaning some calculated values are clearly erroneous and the amount of radiogenic heat flux may be overestimated.

Utilizing the Q-A relationship (equation 1), mantle heat flux (45–60 mW/m^2) plus the radiogenic heat flux (0–4.5 $\mu W/m^3$) times the crust thickness (5–10 km) is the theoretical range for conductive heat flow. The radiogenic component in surface heat flow in the SRP should be approximately 12–40 mW/m^2 (A^*b) based on geochemistry samples and the assigned b of 7.5 ±2.5 km. With the addition of the assigned mantle heat flow of 60 mW/m^2, measured heat flow should be approximately 72–100 mW/m^2 to satisfy the Q-A relationship. Any heat flow measurements outside of this range potentially contain an additional heat input such as advection, refraction, additional radioactivity, or additional mantle heat flux. This is a simplistic analysis of the anomalous heat flux, but is useful to show how and where additional heat inputs are most likely occurring.

The average calculated radiogenic heat production (the model-calculated A) is compared to the whole rock geochemistry heat production (the observed A) values for the SRP (Figure 21). Anomalous heat flux is also examined, calculated as the measured heat flow above the theoretical conductive heat flow limit of 100 mW/m^2 (Figure 22). Finally, anomalous heat flux is compared to model-calculated A and data point locations (Figure 23).

The model-calculated A values are anomalously high throughout the entire SRP, suggesting the whole region may contain an unaccounted-for heat flux component (Figure 21, values >4.5 $\mu W/m^3$). These high, model-calculated A values are located both along the margins and within the SRP. It is unusual, however, that the anomalously high heat flow values are primarily located along the margins and not necessarily co-located with all the high, model-calculated A values. Therefore, these high heat flow sites (Figure 22, values >11 mW/m^2) could be an artifact of grid interpolation. An alternative hypothesis is that the anomalous high heat flow sites are only a small part of the total heat flow signature measured at the surface, on the order of only 0–20 mW/m^2. In the SRP, the average surface heat flow is approximately 100 mW/m^2 (Blackwell 1989), which is the determined theoretical limit of conductive heat flow based on all input values. While the high, model-calculated A suggests a pervasive additional heat flux, it may be undetected because of the high average heat flow of the SRP, or could be an additional

conductive heat flux indistinguishable from the current thermal model. The largest unknown at this time is the radiogenic heat production layer thickness, which in the estimated range of 5 km to 10 km, introduces variability in the heat flow signature of up to 10 mW/m². More information on the radiogenic heat-producing layer thickness would refine the theoretical conductive heat flow limit for the SRP and potentially make the anomalous heat flux signature more resolvable.

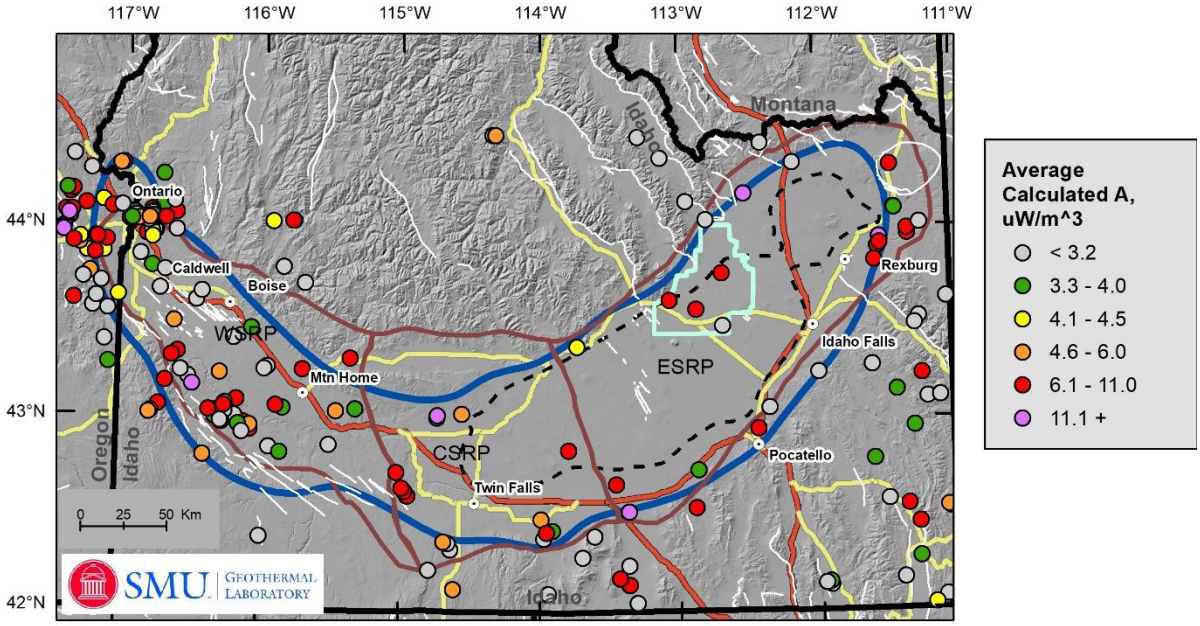

Figure 21. Site-averaged heat production from thermal model.

Each site is the average of 3 values based on thicknesses of 5 km, 7.5 km, and 10 km radiogenic heat-producing layers. Of the 206 sites, 97 contain higher than expected heat production estimates, which suggests additional heat input at these sites.

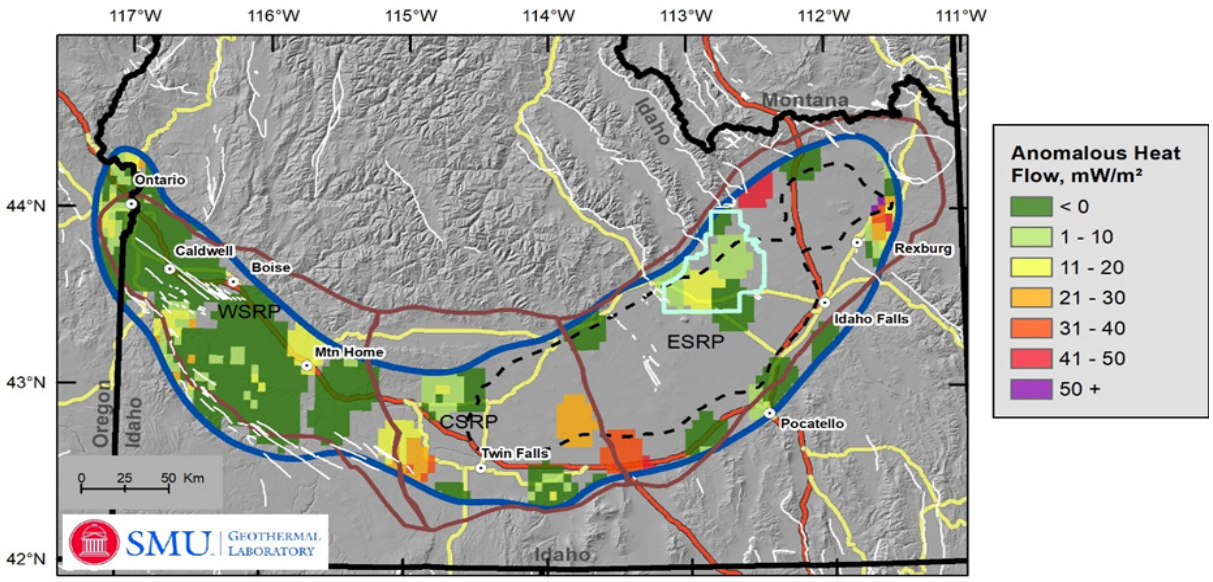

Figure 22. Regional and anomalous heat flow.

Regional heat flow are <100 mW/m² (<0 or dark green areas). Anomalous heat flow are ≥100 mW/m² (1–50+ areas representing 101–150 mW/m²). Much of the WSRP is regional, indicated by the dark green color. Areas above the theoretical conductive heat flow limit of 100 mW/m² could contain an advective heat flux, greater mantle heat flow than modeled, heat refraction, or a combination of all three. Areas with no color have no data.

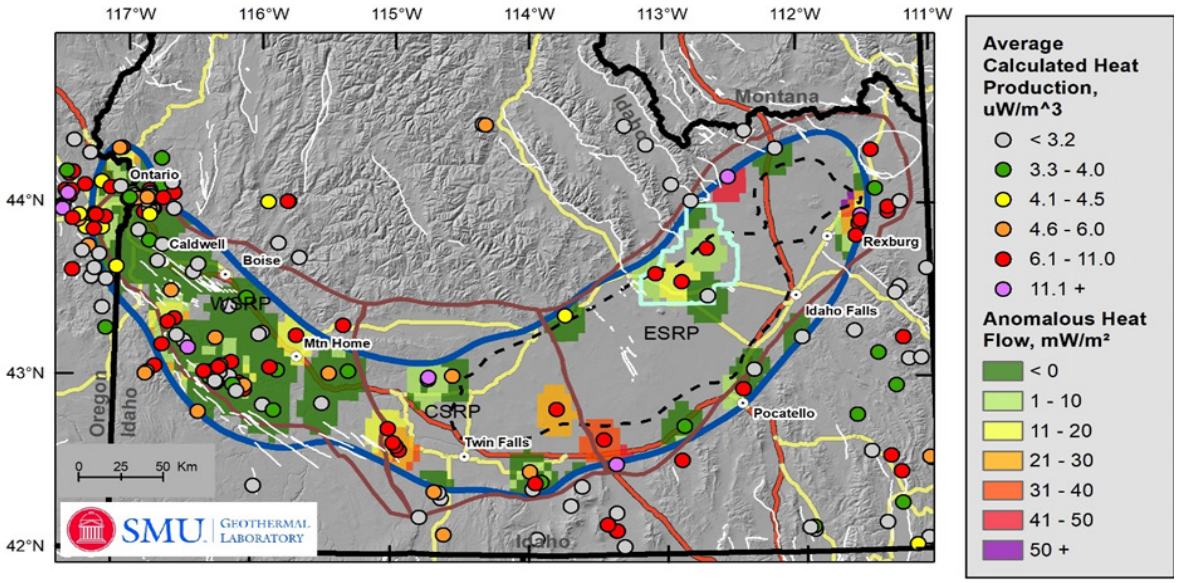

Figure 23. Site-averaged radiogenic heat production values plotted over mapped regional and anomalous heat flow (heat flow >100 mW/m², e.g., 100 + 10 = 110 mW/m²).

Most sites with anomalously high heat production (red and purple dots) correlate to the areas with anomalous heat flow, although some anomalous heat production sites do not correlate to anomalous heat flow sites.

3 Conclusions and Next Steps

3.1 Section 1 Conclusions

This study produced increased resolution of the thermal regime of the WSRP and a better understanding of the thermal regime controls in the greater SRP region. Although limited new well data are available for the CSRP and ESRP regions, the additional well data coverage for WSRP allows for at least one data point within any ~15-km gridding radius circle.

Comparing the geothermal resource evaluation work from the 1970s and 1980s, it is surprising to see that many areas with high temperature wells are still not more deeply assessed by government or private exploration. The areas along the edges of the SRP are complicated, with fault-related fluid flow and complex crustal structure, yet are prospective for both conventional geothermal (power and direct use) and EGS development. The elephant in the room, the ESRPA, is modeled with a high heat source below, yet until additional wells penetrate to depths 1 km or more below it, the proportion of that heat being advectively carried away by the aquifer will remain unknown, along with the full geothermal resource potential.

The thermal potential results from this study show electricity potential (≥150°C) as approximately 44,000 MW_e within the 1 km to 4 km depths. There are potential resources throughout the SRP. The WSRP has at least one data point per 15-km radius, but most of the ESRP lacks data coverage; therefore, although there are several higher-temperature areas in the ESRP, these areas are considered higher risk because of the low data density. Temperature measurements greater than 750 m are accurately predicted by the temperature-at-depth calculations except in areas with known hydrothermal geothermal systems, the Rexburg and Vale areas. At the 3.5 km depth, power potential is 75% greater based on the new temperature-at-depth maps compared to the same area within the 2011 map, even with the removal of the area within the ESRPA.

3.2 Section 2 Conclusions

In this study, we tested the impact on final temperature estimates associated with several steps in our heat flow mapping and temperature-at-depth calculation methodology. No additional data were removed following these additional tests, because these tests showed the heat flow and temperature uncertainty associated with any given test performed was often less than 20%, equivalent to the “B” quality data. This suggests that uncertainty introduced by assumptions in the methodology is primarily less than uncertainty due to measurement error, although several interesting findings came from this temperature uncertainty analysis.

The use of different gridding algorithms produced inconsistent results where there are limited data such as the ESRP, and there were only minor differences in areas with sufficient data coverage such as the WSRP. Still, most gridded areas are within 20% variation, equal to measurement error of “B”-quality data. The ideal scenario for gridding is to produce a study-area-specific semivariogram, but in the SRP there is insufficient data given the spatial extent, which is further complicated by the variable and complex geologic settings. Spline was utilized for resource estimation because of the complete grid coverage, although Kriging would be better to use if there was sufficient data coverage to compute a study-area-specific semivariogram.

Faults have appreciable impact on heat flow within 2.5 km of a Quaternary fault trace, but not at 5 km. Heat flow variability within 2.5 km of faults is mostly within 20%, again equal to "B"-quality data. More data of higher quality and resolution are required to examine the potential fluid flow heat flow patterns that developed after near-fault heat flow data were removed. Only 9 data sites were within 1 km of a fault trace, and only 19 within 2.5 km. The low number of data sites near faults suggests initial processing of data successfully removed individual sites with fluid flow associated with the nearby fault. The larger heat flow pattern, if real, could indicate fluid flow within the fault system, visible on the scale of several kilometers. The presence or lack of this potential fluid flow system is important for exploration within the fault covered portions of the WSRP, CSRP, and ESRP.

The *b* thickness is unknown, but is likely between 5 km and 10 km thickness. Most temperature variability is within 5% at 4 km depth, within the predicted *b* thickness range. Interestingly, though, modeled calculated A is above whole rock geochemistry observed A, suggesting the Q-A relationship is too simple for the SRP thermal regime. Areas with anomalously high heat flow (above 100 mW/m²) or high model calculated A likely have an additional heat component within the measured heat flow not accounted for within the Q-A relationship. This could be additional heat from the mantle (above the model assumed Q_m = 60 mW/m²); a regional, long-term, steady-state fluid flow (i.e., an advective heat component not visible in the temperature logs); a greater *b* thickness; or some combination of these potential inputs. Future geothermal development of the SRP will benefit from determination and incorporation of this additional heat component into the SRP geothermal resource models.

3.3 Additional Data Collection Suggestions

Additional data collection is necessary to further refine assumptions in this model and to resolve remaining questions. Below is a list of suggested future studies, with descriptions of how each would aid in geothermal exploration and thermal regime modeling.

1. New seismic studies that focus on mapping the location and thickness of upper crust in the SRP. These studies would reduce the uncertainty in the utilized *b* thickness value and produce better understanding of the Q-A relationship of the SRP, if this is a valid and applicable relationship for this region.
2. Additional radiogenic heat production measurements co-located with heat flow measurements to make a direct Q-A plot for the WSRP, ESRP, Idaho Batholith, and potentially other surrounding regions. Establishment of several Q-A plots for the study region would examine the variability and applicability of the Q-A relationship for the SRP and would additionally be applicable to the larger northwestern United States, which is impacted by a recent, complex, and volcanism-rich geologic history.
3. Deep drilling in the ESRP that completely penetrates below the ESRPA, records a linear (conductive) gradient for at least 100 m, and possibly drills into the felsic rocks. Such a well would increase heat flow and basement knowledge in a region that lacks sufficient data coverage because of the expansive ESRPA. Suggested well locations are along the south and/or east margin of the ESRPA, such as between Pocatello and Idaho Falls or northwest of Rexburg.

4. Temperature logging of open oil and gas wells in the WSRP. The WSRP shows interesting heat flow patterns associated with the removal of heat flow data within 2.5 km of a Quaternary fault trace, although the changes in heat flow are within measurement error. More detailed temperature well logging could refine the heat flow and add new understanding to possible fluid flow along faults within the WSRP.
5. Deep wells both northwest and northeast of Rexburg would also increase understanding of lithospheric cooling along the Yellowstone Hotspot track that would aid in large-scale, time-dependent, volcanism-age-driven thermal regime models.
6. To the north of the SRP, outside this project focus, is the Central Idaho Basin and Range. This area was cited by Blackwell (1989) as a potential geothermal resource zone, yet no additional data collection or analysis were ever completed. With the focus on EGS and new interest in sedimentary basins for geothermal EGS, this region continues to be a possible area for exploration.
7. The SRP has significant lower-temperature resources in the 50°–150°C range. An energy demand study would highlight how much electricity is needed and in what regions, and may also highlight heating and cooling demands that the lower-temperature resources could fulfill. Additional power potential could be included by performing a low-temperature power generation technology review to justify reducing the minimum temperature cutoff below the current 150°C.

References

Aguirre, Gloria Andrea, Jery R. Stedinger, and Jefferson W. Tester. 2013. "Geothermal resource assessment: A case study of spatial variability and uncertainty analysis for the state of New York and Pennsylvania." Proceedings, Thirty-Eighth Workshop on Geothermal Reservoir Engineering. SGP-TR-198. https://pangea.stanford.edu/ERE/pdf/IGAstandard/SGW/2013/Aguirre.pdf.

Augustine, Chad. 2011. *Updated U.S. Geothermal Supply Characterization and Representation for Market Penetration Model Input*. No. NREL/TP-6A2-47459. National Renewable Energy Laboratory: Golden, CO, United States. https://www.nrel.gov/docs/fy12osti/47459.pdf.

Augustine, Chad. 2016. *Update to Enhanced Geothermal System Resource Potential Estimate*. United States. National Renewable Energy Laboratory: Golden, CO. United States. https://www.osti.gov/servlets/purl/1330935.

Bargar, Keith E., and Terry E.C. Keith. 1999. *Hydrothermal Mineralogy of Core from Geothermal Drill Holes at Newberry Volcano, Oregon*. No. 1578. U.S. Geological Survey. https://pubs.usgs.gov/pp/pp1578/.

Batir, Joseph, Maria Richards, Matthew Hornbach, David Blackwell, and Amanda Kolker. 2020a. "Uncertainty Analysis of Subsurface Temperature Estimates in the Snake River Plain, Idaho." *Geothermal Resources Council Trans*., 44, Abstract and Poster.

Batir, Joseph, Maria Richards, Matthew Hornbach, and David Blackwell. 2020b. *Final Report to Bureau of Land Management on the Shallow EGS Potential of the Snake River Plain.* Under Subcontract NO. XEJ-9-92239-01 under prime Contract NO. DE-AC36-08GO28308 of the Alliance for Sustainable Energy, LLC, Managing and Operating Contractor for the National Renewable Energy Laboratory.

Batir, Joseph, Maria Richards, Matthew Hornbach, David Blackwell, Amanda Kolker, and Al Waibel. 2020c. "Shallow Geothermal Potential of the Snake River Plain." *Geothermal Resources Council Trans*. 44. https://www.geothermal-library.org/index.php?mode=pubs&action=view&record=1034235.

Blackwell, David. 1969. "Heat flow determinations in the northwestern United States." *J. Geophys. Res*. 74: 992–1007.

Blackwell, David. 1971. "The thermal structure of the continental crust." in J.G. Heacock, ed., *The Structure and Physical Properties of the Earth's Crust, Geophys. Mono. Ser. 14*, AGU, Washington D.C., 169–184.

Blackwell, David. 1989. "Regional implications of heat flow of the Snake River Plain, northwestern United States." *Tectonophysics* 164: 323–344.

Blackwell, David, and Robert E. Spafford. 1987. "Experimental methods in continental heat flow." In C.G. Sammis and T.L. Henyey, eds., *Experimental Methods in Physics*. Orlando, FL: Academic Press. 189–226.

Blackwell, David, John Steele, Shari Kelley, and Michael Korosec. 1990. "Heat flow in the State of Washington and thermal conditions in the Cascade Range." *J. Geophys. Res*. 95: 19495–19516. https://agupubs.onlinelibrary.wiley.com/doi/10.1029/JB095iB12p19495.

Blackwell, David D., John L. Steele, and Larry C. Carter. 1991. "Heat Flow Patterns of the North American Continent: A Discussion of the DNAG Geothermal Map of North America." In Slemmons, D.B., E.R. Engdahl, M.D. Zoback, and D.D. Blackwell, eds., *Neotectonics of North America*: Boulder, Colorado, *Geological Society of America*, Decade Map Vol. 1, p. 498.

Blackwell, David, Shari Kelley, and John L. Steele. 1992. "Heat flow modeling of the Snake River Plain, Idaho." U.S. Department of Energy Report for contract DE-AC07-761DO1570, p. 109.

Blackwell, David, and Maria Richards. 2004a. "Geothermal Map of North America." *American Association of Petroleum Geologists* Map, scale 1:6,500,000, Product Code 423.

Blackwell, David, and Maria Richards. 2004b. "The 2004 Geothermal Map of North America; Explanation of Resources and Applications." *Geothermal Resources Council Trans*. 28: 317–320.

Blackwell, David, Petru Negraru, and Maria Richards. 2006. "Assessment of the Enhanced Geothermal System Resource Base of the United States." *Natural Resources Research* 15-4: 283-308. https://link.springer.com/article/10.1007/s11053-007-9028-7.

Blackwell, David, Patrick Stepp, and Maria Richards. 2010. "Comparison and discussion of the 6 km temperature maps of the western US prepared by the SMU Geothermal Lab and the USGS." *Geothermal Resources Council Trans.* 34: GRC1028696.

Blackwell, David, M. Richards, Z. Frone, J. Batir, M. Williams, A. Ruzo, and R. Dingwall. 2011a. *SMU Geothermal Laboratory Heat Flow Map of the Conterminous United States*, U.S. Copyright VA 0001377160. Supported by Google.org. http://www.smu.edu/geothermal.

Blackwell, David, M. Richards, Z. Frone, J. Batir, A. Ruzo, R. Dingwall, and M. Williams. 2011b. "Temperature-at-depth maps for the Conterminous United States and Geothermal Resource Estimates." *Geothermal Resources Council Trans.* 35. http://pubs.geothermal-library.org/lib/grc/1029452.pdf.

Brott, Charles, David Blackwell, and John Mitchell. 1976. "Heat flow in the Snake River Plain region, southern Idaho." *Idaho Dept. Water Resour. Water Info. Bull.* 30–8: 195 p.

Brott, Charles, David Blackwell, and John Mitchell. 1978. "Tectonic implications of the heat flow of the western Snake River Plain, Idaho." *Geological Society of America Bull.* 89: 1697–1707.

Brott, Charles, Davd Blackwell, and John Ziagos. 1981. "Thermal and tectonic implications of heat flow in the Eastern Snake River Plain." *J. Geophys. Res*. 86: 11709–11734. https://agupubs.onlinelibrary.wiley.com/doi/abs/10.1029/JB086iB12p11709.

Colón, Dylan Patrick. 2018. *Understanding the Origins of Yellowstone Hot Spot Magmas through Isotope Geochemistry, High-Precision Geochronology, and Magmatic-Thermomechanical Computer Modeling.* Ph.D. Dissertation at University of Oregon, 321 p.

DeAngelo, Jacob, et al. 2016. "GIS methodology for geothermal play fairway analysis: Example from the Snake River Plain volcanic province." *Proceedings, 41st Workshop on Geothermal Reservoir Engineering,* Stanford University.

Environmental Systems Research Institute. 2019. ArcGIS Desktop Help 10.6 Interpolation Toolset. https://desktop.arcgis.com/en/arcmap/10.6/tools/spatial-analyst-toolbox/an-overview-of-the-interpolation-tools.htm.

Faulds, James, Nicholas Hinz, Gregory Dering, and Drew Siler. 2013. "The Hybrid Model—The most accommodating structural setting for geothermal power generation in the Great Basin, Western USA." *Geothermal Resources Council Trans.* 37: 3–10.

Frone, Zachary, Maria Richards, David Blackwell, and Chad Augustine. 2015. "Shallow EGS Resource Potential Maps of the Cascades." *Proceedings 40th Workshop on Geothermal Reservoir Engineering*, Stanford University. SGP-TR-19. https://pangea.stanford.edu/ERE/pdf/IGAstandard/SGW/2015/Frone.pdf.

Gass, T.E. 1982. "Geothermal heat pumps." *Geothermal Resources Council Bull.* 11:3-8.

Glen, Jonathan MG, Lee Liberty, Erika Gasperikova, Drew Siler, J.W. Shervais, Brent Ritzinger, Noah Athens, and Tait Earney. 2017. "Geophysical investigations and structural framework of geothermal systems in west and southcentral Idaho: Camas Prairie to Mountain Home." *Proceedings of the 42nd Workshop on Geothermal Reservoir Engineering*, Stanford University.

Glen, Johnathan M.G., Lee Liberty, Jared Peacock, Erika Gasperikova, Tait Earney, William Schermerhorn, Drew Siler, John Shervais, and Patrick Dobson. 2018. "A geophysical characterization of the structural framework of the Camas Prairie geothermal system, southcentral Idaho." *Geothermal Resources Council Trans.* 42:466–481. http://pubs.geothermal-library.org/lib/grc/1033924.pdf.

Harper, Thomas Branson. 2018. "Crustal composition beneath southern Idaho: Insights from teleseismic receiver functions." Master of Science Thesis at Boise State University, 98 p.

Hasterok, D. and J. Webb. 2017. "On the radiogenic heat production of igneous rocks." Geoscience Frontiers 8:919-940. https://doi.org/10.1016/j.gsf.2017.03.006.

Hildreth, Wes, Alex N. Halliday, and Robert L. Christiansen. 1991. "Isotopic and Chemical Evidence Concerning the Genesis and Contamination of Basaltic and Rhyolitic Magma Beneath the Yellowstone Plateau Volcanic Field." *Journal of Petrology* 32-1: 63–138.

Hill, D.P. and L.C. Pakiser. 1967. "Seismic-refraction study of crustal structure between the Nevada Test Site and Boise, Idaho." *Geological Society of America Bull.* 78-6: 685–704.

Jordan, Teresa E., et al. 2016. *Low Temperature Geothermal Play Fairway Analysis For The Appalachian Basin: Phase 1 Revised Report*. Cornell University for the U.S. Department of Energy. https://www.osti.gov/servlets/purl/1341349.

Lachenbruch, Arthur H. 1968. "Preliminary geothermal model of the Sierra Nevada." *J. Geophys. Res*. 73-22: 6977–6989.

Lachmar, Thomas, Thomas Freeman, Christopher Sant, Jeffrey Walker, Joseph Batir, John Shervais, James Evans, Dennis Nielson, and David Blackwell. 2017. "Effect of an 860-m thick, cold, freshwater aquifer on geothermal potential along the axis of the eastern Snake River Plain, Idaho." *Geothermal Energy* 5–28. doi:10.1186/s40517-017-0086-8. https://geothermal-energy-journal.springeropen.com/articles/10.1186/s40517-017-0086-8.

Lachmar, Thomas, Thomas Freeman, James Kessler, Joseph Batir, James Evans, Dennis Nielson, John Shervais, Xiwei Chen, Douglas Schmitt, David Blackwell. 2019. "Evaluation of the geothermal potential of the western Snake River Plain based on a deep corehole on the Mountain Home AFB near Mountain Home, Idaho." *Geothermal Energy* 7-26. https://geothermal-energy-journal.springeropen.com/articles/10.1186/s40517-019-0142-7.

Lindholm, Gerald F. 1996. *Summary of the Snake River Plain regional aquifer-system analysis in Idaho and eastern Oregon*. No. 1408-A. U.S. Government Printing Office. https://pubs.usgs.gov/pp/1408a/report.pdf.

Ludington, Steve, Barry Moring, Robert Miller, James Evans, Paul Stone, Arthur Bookstrom, Constance Nutt, David Bedford, Gordon Haxel, Melanie Hopkins, and Katheryn Flynn. 2005. *Preliminary integrated geologic map databases for the United States: Western States: California, Nevada, Arizona, Washington, Oregon, Idaho, and Utah.* United States Geological Survey. http://pubs.usgs.gov/of/2005/1305/.

Machette, M.N., K.M. Haller, R.L. Dart, and S.B. Rhea. 2003. "Quaternary fault and fold database of the United States." *U.S. Geological Survey Open-File Report 03-417*.

McLing, Travis, Richard Smith, Robert Smith, David Blackwell, Robert Roback, and Andrus Sondrup. 2016. "Wellbore and groundwater temperature distribution eastern Snake River Plain, Idaho: Implications for groundwater flow and geothermal potential." *Journal of Volcanology and Geothermal Research* 320: 144–155.

McCurry, Michael, Travis McLing, Richard Smith, William Hackett, Ryan Goldsby, William Lochridge, Robert Podgorney, Thomas Wood, David Pearson, John Welhan, Mitch Plummer. 2016. "Geologic Setting of the Idaho National Laboratory Geothermal Resource Research Area." *Proceedings, 41st Workshop on Geothermal Reservoir Engineering: Stanford University, Stanford California, SGP-TR-209*. https://pangea.stanford.edu/ERE/pdf/IGAstandard/SGW/2016/Mccurry.pdf.

National Geothermal Data System, SMU Node, 2014. geothermal.smu.edu/GTDA

Pierce, Kenneth and Lisa Morgan. 2009. “Is the track of the Yellowstone hotspot driven by a deep mantle plume?—Review of volcanism, faulting, and uplift in light of new data.” *Journal of Volcanology and Geothermal Research* 188: 1–25.

Podgorney, R., Neil Snyder, and M. Roy. 2016. “A Snake River Plain Field Laboratory for Enhanced Geothermal Systems: an Overview of the Snake River Geothermal Consortium’s Proposed FORGE Approach and Site.” *Proceedings, 41st Workshop on Geothermal Reservoir Engineering*, Stanford University.

Richards, Maria, David Blackwell, Mitchell Williams, Zachary Frone, Ryan Dingwall, Joseph Batir, and Cathy Chickering. 2012. “Proposed Reliability Code for Heat Flow Sites.” *Geothermal Resources Council Trans.* 36: 211–218.

Rodgers, David W., H. Thomas Ore, Robert T. Bobo, Nadine McQuarrie, Nick Zentner, B. Bonnichsen, C. M. White, and M. McCurry. 2002. “Extension and subsidence of the eastern Snake River Plain, Idaho.” In Bill Bonnichsen, C.M. White, and Michael McCurry, eds., *Tectonic and Magmatic Evolution of the Snake River Plain Volcanic Province:* Idaho Geological Survey Bulletin 30: 121–155.

Roy, Robert, David Blackwell, and Francis Birch. 1968. “Heat generation of plutonic rocks and continental heat flow provinces.” *Earth and Planetary Science Letters* 5:1–12.

Shervais, John, Gaurav Shroff, Scott Vetter, Scott Matthews, Barry Hanan, and James McGee. 2002. “Origin and Evolution of the Western Snake River Plain: Implications for Stratigraphy, Faulting, and the Geochemistry of Basalts Near Mountain Home, Idaho” In Bill Bonnichsen, C.M. White, and Michael McCurry, eds., *Tectonic and Magmatic Evolution of the Snake River Plain Volcanic Province:* Idaho Geological Survey Bulletin 30: 343–361.

Shervais, John, et al. 2012. “Hotspot: The Snake River Geothermal Drilling Project—Initial Report.” *Geothermal Resources Council Trans.* 36: 767–772.

Shervais, John, et al. 2013. “First results from HOTSPOT: the Snake River Plain scientific drilling project, Idaho, USA.” *Scientific Drilling* 15.

Shervais, John, et al. 2015. “Snake River Plain Play Fairway Analysis–Phase 1 Report.” *Geothermal Resources Council Trans.* 39: 761–769.

Shervais, John, et al. 2020. “Play Fairway Analysis in Geothermal Exploration: The Snake River Plain Volcanic Province.” *Proceedings, 45st Workshop on Geothermal Reservoir Engineering*, Stanford University.

Smith, Jared. 2016. *Analytical and geostatistical heat flow modeling for geothermal resource reconnaissance applied in the Appalachian Basin*. PhD Dissertation, Cornell University, Ithaca, NY.

Smith, J., and F. Horowitz. 2016. “Seismic Risk Map Creation Methods.” In *Low Temperature Geothermal Play Fairway Analysis for the Appalachian Basin: Final Phase 1 Research Report*. U.S. Department of Energy. DEE0006726.

Sparlin, M.A. 1981. *Crustal structure of the eastern Snake River Plain determined from ray-trace modeling of seismic refraction data*, M.S. Thesis, Purdue University, W. Lafayette, IN, 62 pp.

Stutz, George R., Mitchell Williams, Zachary Frone, Timothy J. Reber, David Blackwell, Teresa Jordan, and Jefferson W. Tester. 2012. "A well by well method for estimating surface heat flow for regional geothermal resource assessment." *Proceedings, 37th Workshop on Geothermal Reservoir Engineering*, Stanford University. *SGP-TR-194*.

Stutz, George R., Elaina Shope, Gloria Andrea Aguirre, Joseph Batir, Zachary Frone, Mitchell Williams, Timothy J. Reber, Calvin A. Whealton, Jared D. Smith, Maria C. Richards, David D. Blackwell, Jefferson W. Tester, Jery R. Stedinger, and Teresa E. Jordan. 2015. "Geothermal energy characterization in the Appalachian Basin of New York and Pennsylvania." *Geosphere* 11-5: 1291–1304.

Tester, Jefferson W., et al. 2006. *The Future of Geothermal Energy: Impact of Enhanced Geothermal Systems (EGS) on the United States in the 21st Century*. Massachusetts Institute of Technology, DOE Contract DE-AC07-05ID14517 Final Report, 374 p. https://www.ourenergypolicy.org/wp-content/uploads/2012/05/future_of_geothermal_energy.pdf.

Troch, Juliana, Ben S. Ellis, Darren F. Mark, Ilya N. Bindeman, Adam J. R. Kent, Marcel Guillong, and Olivier Bachmann. 2017. "Rhyolite Generation prior to a Yellowstone Supereruption: Insights from the Island Park-Mount Jackson Rhyolite Series." *Journal of Petrology* 58-1: 29–52.

U.S. Geological Survey. 2015. *Snake River Plain Basin-fill aquifer system*, vector digital data, 2nd Edition: Reston, VA. https://water.usgs.gov/GIS/metadata/usgswrd/XML/snake_river_plain_aquifer_system.xml#stdorder.

Utah State University. 2014a. Project HOTSPOT: Kimama Well Borehole Geophysics Database. http://gdr.openei.org/submissions/291.

Utah State University. 2014b. Project HOTSPOT: Kimberly Well Borehole Geophysics Database. http://gdr.openei.org/submissions/283.

Utah State University. 2014c. Project HOTSPOT: Mountain Home Well Borehole Geophysics Database. http://gdr.openei.org/submissions/284.

Whitehead, R.L. 1992. "Geohydrologic framework of the Snake River plain regional aquifer system, Idaho and eastern Oregon." U.S. Geological Survey. Professional Paper 1408-B. doi:10.3133/pp1408B. https://pubs.er.usgs.gov/publication/pp1408B.

Wood, Spencer, and Drew Clemens. 2002. “Geologic and tectonic history of the western Snake River Plain, Idaho and Oregon.” In Bill Bonnichsen, C.M. White, and Michael McCurry, eds., Tectonic and Magmatic Evolution of the Snake River Plain Volcanic Province: Idaho Geological Survey Bulletin 30: 69–103. https://idwr.idaho.gov/files/projects/north-ada-county/199807-WOODCLEM-2002.pdf.

Appendix A. Complete Heat Flow Data Set

An accompanying spreadsheet includes information on all 926 data sites examined to calculate heat flow for the SRP region. The first 206 are the data sites utilized for heat flow and temperature-at-depth calculation, and they are labeled as being included for the heat flow study. The remaining 720 sites are those that were not utilized for this study. Notes for each data point are included in the "Notes" column, which highlight reasoning for keeping or discarding data.

Appendix B. Generalized Lithology Logs

This appendix includes discussion of the generalized lithology logs developed to calculate heat flow for well sites with only temperatures and depth measurements. The following lithology logs are developed based on the available information for each area. The five generalized lithology columns are WSRP, Mountain (Mtn.) Home, CSRP, ESRP, and southeast of the SRP (SE ID). The thermal conductivity values associated with each lithology classification rock type are in the main report in Table 3 ("Assigned Conductivities Based on Rock Type").

For future research and projects, more refined lithology models would improve thermal regime estimates, especially for geothermal projects focused on deeper, higher-temperature resources. The most significant improvement to the lithology models would come from an accurate estimate of the depth to felsic rock (i.e., basement), ideally through seismic studies, or developed through gravity and magnetic inversion as well as deeper drilling.

Abbreviations for each rock type are as follows:

UNCON	unconsolidated sediments
SH	shale
SS	sandstone
SS/SH	interbedded sandstone and shale
SLT/SH	interbedded siltstone and shale
LS	limestone
SH/LS	interbedded shale and limestone
LS/SS	interbedded limestone and sandstone
SED	undifferentiated/general sedimentary rocks
RHY	rhyolite
BAS	basalt
VOLC	undifferentiated/general volcanic rocks
BAS/SH	interbedded basalt and shale
BAS/SED	interbedded basalt and undifferentiated/general sedimentary rocks
RHY/BAS/SED	interbedded rhyolite, basalt, and undifferentiated/general sedimentary rocks

B.1 Western Snake River Plain Generalized Lithology

The generalized lithology for the WSRP (Table 8) is a combination of work from past studies within the sedimentary basin, previous cross sections (Shervais et al. 2002; Wood and Clemens 2002; Whitehead 1992), and newly collected lithology data for the area. The deepest section of the WSRP lithology model includes high standard deviations and is greater than the known sedimentary section thickness. This deepest section is built from previous cross sections that suggest thick deep basalts related to the Columbia River Basalts, and an equally thick section of sediment below, although no wells in the center of the basin have ever been drilled to this sedimentary section. This is a key area of potential improvement for future studies. For the thermal models, the lithology sections are proportionally scaled to the wells so that the sedimentary section thickness equals the assigned basement depth as a way to limit potential error associated with unknown lithology thicknesses.

Table 8. WSRP Generalized Lithology

Rock Type / Unit	Thickness (m): Minimum	Maximum	Assumed	Std. Dev.	Subsurface Depth (m)	Thermal Conductivity (W/m*K)
UNCON	2	18	7	5	7	1.2
SS/SH	15	79	60	19	67	2
BAS	62	62	62	0	129	1.7
SS/SH	19	152	65	53	194	2
BAS	15	15	15	0	209	1.7
SS/SH	39	201	112	67	321	2
BAS	53	53	53	0	374	1.7
SS/SH	77	175	126	49	500	2
BAS/SH	15	240	114	92	614	1.6
SED	3	284	95	115	710	1.9
BAS/SH	2	174	45	54	755	1.5
SH	49	350	179	128	934	1.2
BAS/SH	7	189	80	55	1014	1.5
SED	32	526	251	179	1265	1.8
BAS/SH	18	599	233	210	1498	1.5
SED	3	714	299	274	1797	1.8
BAS/SH	15	858	254	300	2051	1.5
SED	250	277	264	14	2314	1.8
BAS/SH	48	505	206	158	2520	1.5
SED	37	1224	567	493	3088	1.8
VOLC	1	874	213	298	3301	1.4
SS/SH	305	712	550	176	3851	1.9
BAS/SH	2	1380	192	341	4043	1.4
SS/SH	287	1082	605	344	4647	1.9
VOLC	375	1064	671	290	5318	1.4
SED	193	193	193	0	5511	1.75
BAS	0	1914	1914	1500	7425	1.4
SED	0	1953	1675	1500	9100	1.75

B.2 Mountain Home Generalized Lithology

The Mtn. Home generalized lithology (Table 9) is built following the lithology logs from the Mtn. Home AFB #1 and the Mtn. Home #2B drilled as part of the *HOTSPOT* Project. The lithology and thermal conductivity were iteratively refined to accurately estimate temperature within the Mtn. Home #2B and Mtn. Home AFB #1 wells. Other wells in the general vicinity of Mtn. Home are included within this lithology section.

Table 9. Mtn. Home Generalized Lithology

Rock Type / Unit	Thickness (m):				Subsurface Depth (m)	Thermal Conductivity (W/m*K)
	Minimum	Maximum	Assumed	Std. Dev.		
UNCON	3	15	9	5	9	1.2
BAS	213	250	213	64	223	1.6
SED	640	700	640	84	863	1.7
BAS	152	175	152	20	1015	1.4
SED	152	200	152	41	1167	1.6
BAS	61	75	61	10	1228	1.3
SED	30	50	30	11	1259	1.6
BAS/SED	305	350	305	41	1564	1.4
BAS	274	300	274	20	1838	1.3

B.3 Central Snake River Plain Generalized Lithology

The CSRP generalized lithology (Table 10) is built following the lithology logs for the Kimberly well drilled as part of the *HOTSPOT* Project with other local shallow lithology logs used to confirm continuity of the upper lithology sections. This is a large area, with the Kimberly well the only deep well in the section.

Table 10. CSRP Generalized Lithology

Rock Type / Unit	Thickness (m):				Subsurface Depth (m)	Thermal Conductivity (W/m*K)
	Minimum	Maximum	Assumed	Std. Dev.		
UNCON	3	23	14	7	14	1.2
BAS	7	110	59	34	73	1.6
RHY/BAS/SED	12	200	80	62	153	1.75
BAS	30	258	144	114	298	1.7
SED	52	55	53	1	351	2
BAS	57	112	84	27	436	1.5
RHY/BAS/SED	8	289	75	74	511	1.7
RHY	3	337	169	136	680	1.75
BAS/SED	20	596	211	200	891	1.5
RHY	44	1531	663	632	1554	1.75

B.4 Eastern Snake River Plain Generalized Lithology

The ESRP generalized lithology (Table 11) is built following wells located within the INL boundary and the Kimama well in the southwest portion of this general lithology zone. There are several small lacustrine sediment beds that are intersected in most of the deepest wells in the ESRP, although it is unclear how continuous these beds are. There is also no clear demarcation between mafic and felsic volcanism in the central part of the ESRP. Therefore, this generalized lithology is comparatively simple, but also could use improvements from deeper drilling or seismic studies.

Table 11. ESRP Generalized Lithology

Rock Type / Unit	Thickness (m): Minimum	Maximum	Assumed	Std. Dev.	Subsurface Depth (m)	Thermal Conductivity (W/m*K)
UNCON	1	3	2	1	2	1.2
BAS	100	300	150	85	152	1.6
SED	0	100	50	31	202	1.7
BAS	152	600	200	187	402	1.5
SED	0	100	75	31	477	1.6
BAS	61	75	200	62	677	1.5
SED	0	50	50	12	727	1.6

B.5 Southeastern Idaho Generalized Lithology

The SE ID generalized lithology section (Table 12) is built from deep oil and gas exploration wells drilled south and east of the SRP, along the Idaho-Wyoming border. The majority of the wells used for building this lithology section came from the National Geothermal Data System (National Geothermal Data System 2014), and is clearly a different geologic setting. Still, this lithology section and the wells in the southeast region of Idaho are used for regional context for heat flow and thermal regime mapping.

Table 12. Southeastern Idaho Generalized Lithology

Rock Type / Unit	Thickness (m): Minimum	Maximum	Assumed	Std. Dev.	Subsurface Depth (m)	Thermal Conductivity (W/m*K)
UNCON	1	18	8	6	8	1.2
VOLC	21	58	38	12	46	1.6
SED	43	213	175	59	222	2
LS	110	216	163	53	385	2.3
SH/LS	2	265	96	85	481	1.9
RHY	6	265	135	129	616	1.75
LS/SS	12	115	57	37	673	2.4
BAS/SED	65	364	157	121	830	2
SH/LS	37	448	195	125	1026	1.8
SLT/SH	487	495	491	4	1517	1.7
SH/LS	54	605	237	177	1754	1.8
SED	34	549	218	168	1972	1.9
LS	60	951	355	276	2327	2.3
SED	36	1132	291	263	2617	1.85
LS	7	1411	409	321	3026	2.3
SED	27	835	321	238	3347	1.85
LS	55	1528	388	480	3734	2.25
SED	18	1708	252	336	3987	1.85
LS	94	629	240	185	4227	2.25
SED	26	1903	342	494	4568	1.85
SH/LS	2	2563	326	488	4894	1.75
SED	0	652	222	153	5116	1.85
LS	55	1706	566	432	5683	2.25
SED	31	814	226	209	5908	1.85
SH/LS	0	2286	317	383	6225	1.75
SED	18	303	177	91	6402	1.85
SH/LS	50	1419	431	440	6832	1.75
SED	5	1928	244	337	7077	1.85
LS	54	626	271	223	7347	2.3
SED	123	1928	738	712	8085	1.85
SH/LS	5	784	189	232	8274	1.75

Appendix C. Temperature-Depth Logs of the Snake River Plain Regions

Deep temperature logs and BHT data are displayed in this appendix for the WSRP, CSRP, and ESRP (Figure 24–Figure 26). There are many similar geothermal gradients at depth, but with visible variability. Temperature data are displayed here as reference for analysis. The Bostic 1-A well is on the border of the WSRP and CSRP and could fit into either regional plot. Similarly, the Kimama well is on the border of the CSRP and the ESRP and could fit into either plot. The Bostic 1-A, Kimberly, and Kimama wells are all plotted on the CSRP temperature-depth plot and display, in part, the breadth of temperature log variability throughout the SRP.

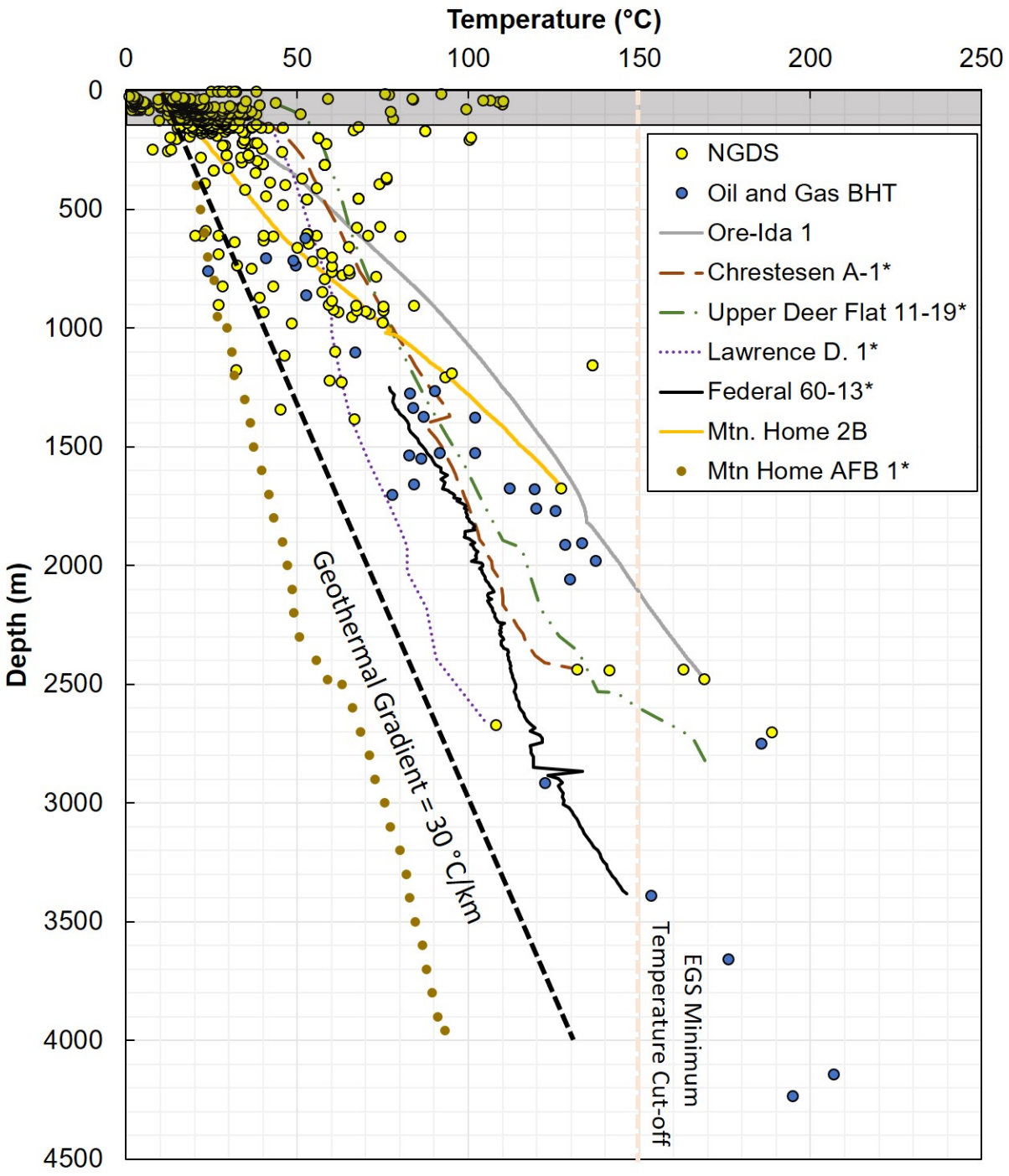

Figure 24. Temperature data for the WSRP.

Temperature logs with an asterisk have an unknown history and may not be at equilibrium. Note that many of the data are above the continental average geothermal gradient of 30°C/km. Data in the gray box are shallower than 125 m depth and are not utilized for heat flow or temperature-at-depth calculations.

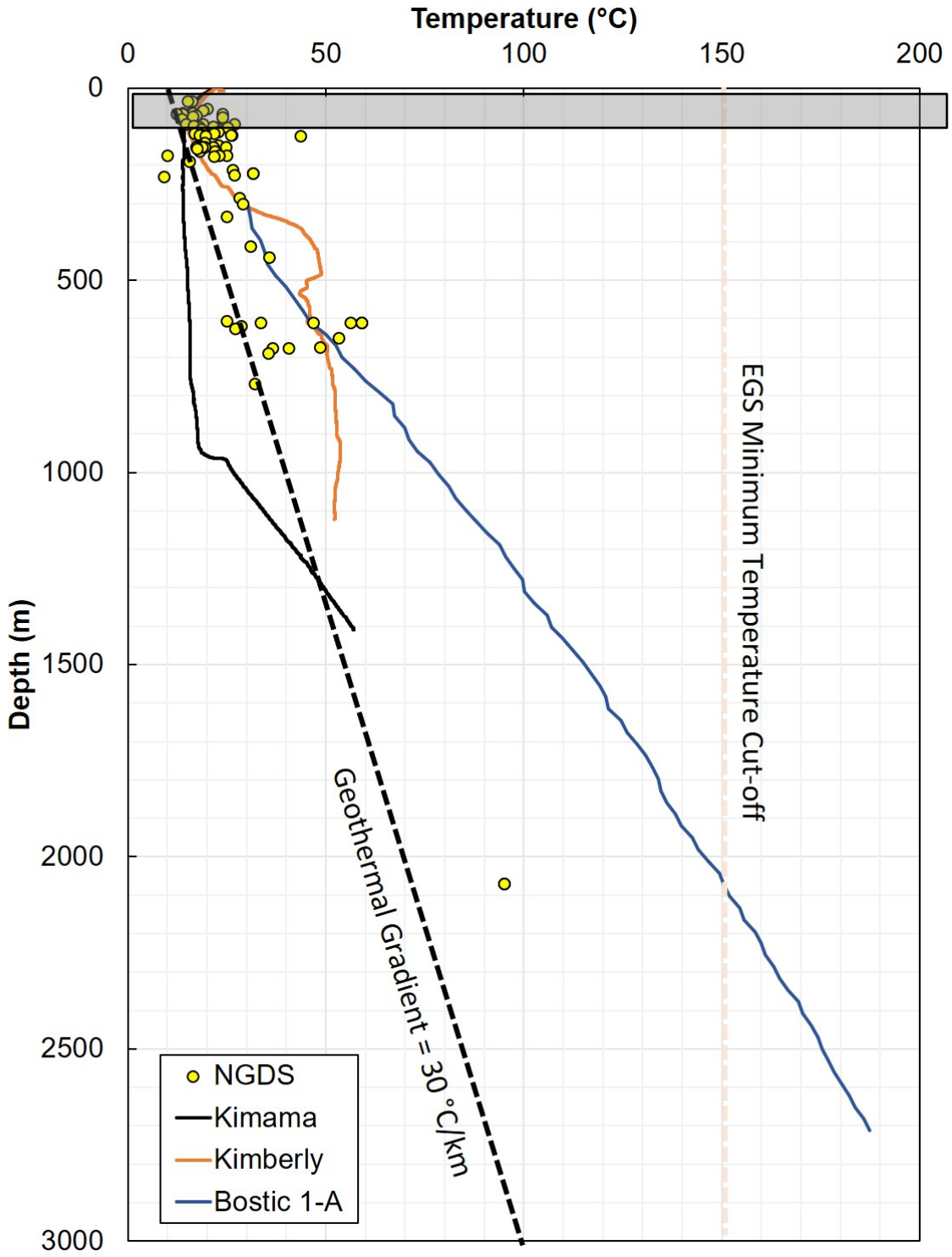

Figure 25. Temperature data for the CSRP.

The wells displayed show the amount of variability in the thermal regime with depth and the ability for fluid flow to impact the temperature logs. Data in the gray box are shallower than 125 m depth and are not utilized for heat flow or temperature-at-depth calculations.

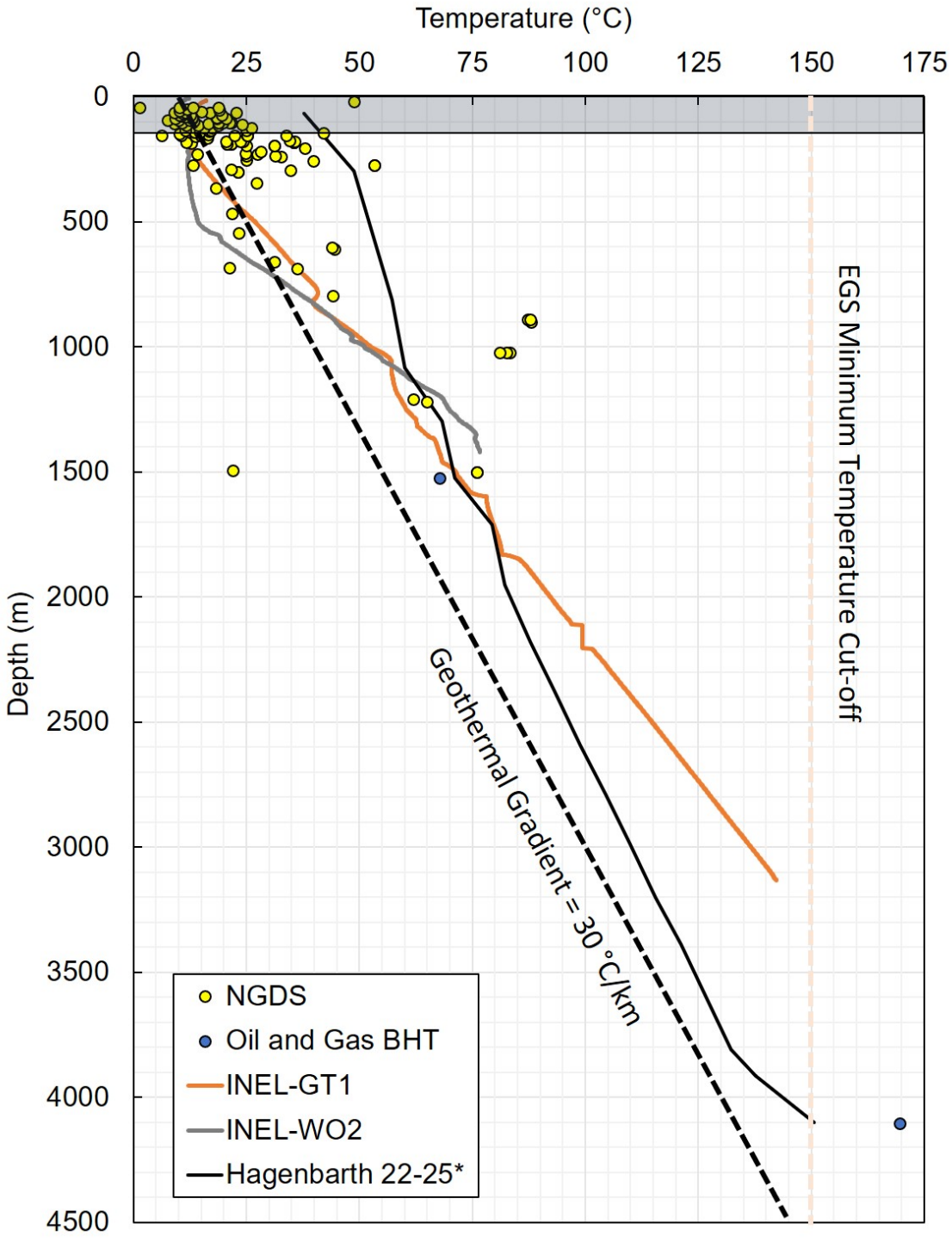

Figure 26. Temperature data for the ESRP.

Temperature logs display conductive gradients below the ESRPA, although with some additional fluid flow zones. Data in the gray box are shallower than 125 m depth and are not utilized for heat flow or temperature-at-depth calculations.